Dissipation and geometry in nonlinear quantum transports of multiband electronic systems

Yoshihiro Michishita and Naoto Nagaosa

Phys. Rev. B **106**, 125114 — Published 12 September 2022

DOI: 10.1103/PhysRevB.106.125114

Dissipation and geometry in nonlinear quantum transports of multiband electronic systems

Yoshihiro Michishita[1,*] and Naoto Nagaosa[1,2,†]

[1] *RIKEN Center for Emergent Matter Science (CEMS), Wako, Saitama 351-0198, Japan*
[2] *Department of Applied Physics, The University of Tokyo, Bunkyo, Tokyo 113-8656, Japan*

(Dated: August 31, 2022)

Nonlinear responses in condensed matter attract recent intensive interest because they provide rich information about the materials and hold the possibility of being applied in diodes or high-frequency optical devices. Nonlinear responses are often closely related to the multiband nature of the system, which can be taken into account by the geometric quantities such as the Berry curvature, as shown in the nonlinear Hall effect. Theoretically, the semi-classical Boltzmann treatment or the reduced density matrix method have been often employed, in which the effect of dissipation is included through the relaxation time approximation. In the diagrammatic method, the relaxation is treated through the imaginary part of the self-energy of the Green function and the consequent broadening of the spectral function for the integration over the real frequency. Therefore, the poles of the Green function do not play an explicit role when there is finite dissipation. In this paper, in stark contrast to this conventional picture, we show that the poles of the Green function determine mainly the nonlinear response functions with dissipation, which leads to the terms with the Fermi distribution function of complex argument and results in the dissipation-induced geometric term. Furthermore, we elucidate the geometric origin of the nonreciprocal conductivity, which is related to the Berry curvature generalized to the higher derivative. Finally, we derive the analytical results on the geometric terms of the nonlinear conductivities in the type-I and type-II Weyl Hamiltonian to demonstrate their crucial roles.

I. INTRODUCTION

Recently, nonlinear response in the bulk systems in condensed matter physics has been intensively studied, especially in the context of the higher-harmonic generations[1–6], nonlinear Hall effect[7–11], photovoltaic effect[12–16], and non-reciprocal transport[17–26] because they have the information on the symmetry of material and have the possibility of the application to devices. For example, we can detect the parity-breaking of the bulk through the detection of the second harmonic generation[1–3]. Furthermore, the photovoltaic effect in bulk has the possibility of application to high-frequency rectification devices[16]. Moreover, the large non-reciprocality was found in the superconductors[21–23] and can be applied to the diode devices.

In the linear conductivity, the effect of dissipation and multi-band contribution are usually separated, such as the anomalous quantum Hall effect, which can be described by the Berry curvature and is not affected by dissipation. On the other hand, in the nonlinear conductivity, both dissipation and multi-band contribution intertwine the novel transport. For example, the Berry curvature dipole term is proportional to the lifetime, which is the inverse of the strength of dissipation, while it is also proportional to the Berry curvature[27–29]. Moreover, it has been pointed out in Ref.[18] that, for the nonreciprocal current under the time-reversal symmetry (TRS), both dissipation and multi-band are necessary. Therefore, it is essential to properly analyze the effect of dissipation on the multi-band contribution in the nonlinear conductivities.

In most previous studies, the nonlinear response has been commonly studied by the semi-classical Boltzmann (SCB) treatment[7, 27, 28, 30] or the reduced density matrix (RDM) method[4, 31–35]. In these methods, it is not easy to consider the effect of dissipation rigorously. Therefore, we usually use the relaxation time approximation (RTA) to include the dissipation or calculate each relaxation time for various scatterings[27, 28], such as the side-jump and skew scattering. RTA has the problem that it breaks the gauge invariance between the velocity gauge and the length gauge[31, 36], and it cannot describe the proper relaxation when considering the finite input frequency[36], while it well describes the relaxation when considering the DC input[36].

In the microscopic diagrammatic theory, the relaxation is treated by the imaginary part of the self-energy of the Green's function and the vertex corrections. The former also leads to the broadening of the spectral function, which appears in the integration over the real frequency. The reason for this integration path is to avoid the poles of the Fermi distribution function at Matsubara frequencies, but those contributions are small for nonlinear responses, as will be shown later. Therefore, the poles of the Green's with imaginary parts and the Fermi distribution function with complex argument play an important role. In the previous studies, while the relaxation of the non-equilibrium states can be considered through the RTA, the effect of the broadening of the distribution function cannot be captured.

In this paper, we analyze the effect of the broadening of

* yoshihiro.michishita@riken.jp
† nagaosa@riken.jp

the spectral function on the nonlinear transport. We elucidate that the broadening of the spectral function results in the shift of the Fermi distribution function (DF) to the imaginary direction and the Matsubara term, which cannot be described by the SCB treatment or the RDM method. Furthermore, the shift of the Fermi DF to the imaginary direction gives the novel dissipation-induced geometric terms. For example, the Christoffel symbol term appears in second-order nonlinear transport and gives the multi-band correction to the nonlinear Drude term. We note that this Christoffel symbol term is completely different from Ref.[37], in which it appears under the magnetic field. We also elucidate the geometric origin of the non-reciprocal conductivity, which is related to the Berry curvature generalized to higher derivatives and is also a dissipation-induced geometric term. Moreover, we analytically derive the geometric term in the Weyl Hamiltonian for the type-I and type-II cases. We show that the chemical potential dependence of the nonlinear Hall conductivity for each case is entirely different, and therefore, the observation of such chemical potential dependence can lead to the detection of the Weyl points and their type. Especially for the type-I case, we also show that we can estimate the relaxation time in the material from this observation.

In the following, we derive the shift of the Fermi DF to the imaginary direction and the Matsubara terms from the Green function methods[36, 38]. First, we derive them in the linear conductivity to illustrate the formulation in section II. We show the shift of the Fermi DF results in the quantum metric term at the Fermi surface. In section III, we extend the results in the linear response to the nonlinear transport and derive the geometrical terms, such as the Christoffel symbol term and the generalized Berry curvature term. Then, we numerically calculate it in a model for transition metal dichalcogenides and show its dissipation-strength and chemical potential dependence. In section IV, we derive the analytical results of the geometric terms such as the Berry curvature dipole term and the Christoffel symbol term for the type-I and type-II Weyl Hamiltonian. In section V, we summarize our results.

II. DISSIPATIVE GEOMETRY IN LINEAR CONDUCTIVITY

Before considering nonlinear conductivity, we first analyze the dissipation effect in linear conductivity. Although the methods we use in this paper are not so effective in linear conductivity, the analysis in linear conductivity is pedagogical and helps us understand the results in nonlinear conductivity.

A. Formulation

In this paper, we include the dissipation effect via the imaginary part of the single-particle self-energy and calculate the conductivity using Green function methods. Throughout this paper, we ignore the momentum and frequency dependence of the dissipation and suppose the dissipation strength is the same for all bands. This assumption and approximation are justified when considering the impurity scattering, independent of the momentum transfer, under the first-order Born approximation. It is also justified to ignore the vertex correction because here we ignore the momentum dependence of the self-energy and satisfy the Ward-Takahashi equation. Under these approximations and assumptions, the single-particle Green function has the same eigenstate as the Hermitian part of the effective Hamiltonian $\mathcal{H}_{\rm eff} = \mathcal{H}_0 + {\rm Re}\Sigma^R$. We also set $e = k_B = \bar{h} = 1$ throughout this paper.

First, we analyze the dissipation effect through the distribution function in the linear conductivity, and focus on the symmetric part of the linear DC conductivity $\sigma^{\alpha\beta}_{DC} = (\sigma^{\alpha;\beta} + \sigma^{\beta;\alpha})/2$ for simplicity.[39] $\alpha(\beta)$ in $\sigma^{\alpha;\beta}$ represents the output(input) direction. $\sigma^{\alpha\beta}_{DC}$ can be written in the Green function methods with the band-indices n, m as,

$$\sigma^{\alpha\beta}_{\rm DC} = \sum_{\boldsymbol{k}} \int_{-\infty}^{\infty} \frac{d\omega}{2\pi} {\rm Re} \sum_{nm} \mathcal{J}^{\alpha}_{nm} G^R_m \mathcal{J}^{\beta}_{mn} \big(G^R_n - G^A_n\big) \frac{\partial f}{\partial \omega} \quad (1)$$

where $\mathcal{J}^{\alpha} = \partial^{\alpha}\mathcal{H}_{\rm eff}$, $\partial^{\alpha} = \partial/\partial k^{\alpha}$, $\mathcal{O}_{nm} = \langle n|\mathcal{O}|m\rangle$, $\mathcal{O}_n = \mathcal{O}_{nn}$, $|n\rangle$ is the eigenstates of $\mathcal{H}_{\rm eff}$, and $f(\omega)$ is the Fermi distribution function. Throughout this paper, we omit writing the momentum dependence of the function, such as $\mathcal{J}, \epsilon_n, G^{R(A)}_n$, and the frequency dependence of the Green function. In the limit $|\omega| \to \infty$, the integrand is proportional to $1/|\omega|^3$, and therefore, the integration $\int_{-\infty}^{\infty} d\omega/2\pi$ is equivalent to the contour integral $\oint_C d\omega/2\pi$.(along the closed loop C in Fig. 1.) For this integral, we should consider the poles of the advanced Green function (green cross marks in Fig. 1.) and the Matsubara frequencies from the Fermi distribution function (red cross marks in Fig. 1.). Then, Eq. (1) can be written as,

$$\sigma^{\alpha\beta}_{\rm DC} = \sigma^{\alpha\beta}_{\rm M} + \sigma^{\alpha\beta}_{\rm G} \quad (2)$$

$$\sigma^{\alpha\beta}_{\rm M} = {\rm Re} \sum_{\boldsymbol{k}} \frac{i}{2\beta} \sum_{nm} \sum_{\omega_M>0} (\mathcal{J}^{\alpha}_{nm}\mathcal{J}^{\beta}_{mn} + \mathcal{J}^{\beta}_{nm}\mathcal{J}^{\alpha}_{mn}) \times \Big[\frac{\partial}{\partial\omega}\Big(G^R_m(G^R_n - G^A_n)\Big)\Big]_{i\omega_M} \quad (3)$$

$$\sigma^{\alpha;\beta}_{\rm G} = {\rm Re} \sum_{\boldsymbol{k}} \sum_{n} \Big[\mathcal{J}^{\alpha}_n \mathcal{J}^{\beta}_n \tau + i \sum_{m\neq n} \frac{(\mathcal{Q}^{\alpha\beta}_{D;n,m} + \mathcal{Q}^{\beta\alpha}_{D;n,m})}{2} \times (\epsilon_{nm} + 2i\eta)\Big] \Big(-\frac{\partial f}{\partial\omega}\Big)_{\epsilon_n + i\eta}, \quad (4)$$

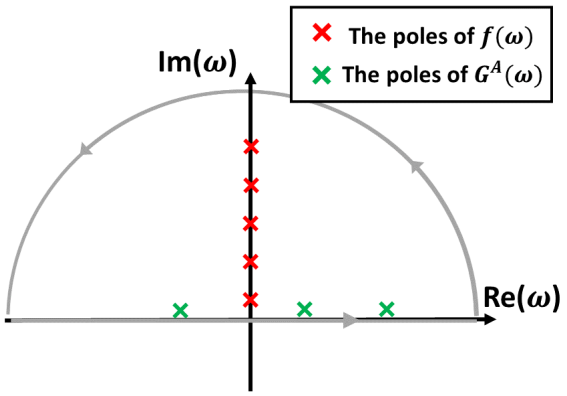

FIG. 1. Path integration Path integration in the DC limit.

with

$$\mathcal{Q}^{\alpha\beta}_{D;n,m} = \frac{\mathcal{J}^{\alpha}_{nm}\mathcal{J}^{\beta}_{mn}}{(\epsilon_{nm}+2i\eta)^2}, \tag{5}$$

where $\omega_M = (2M+1)\pi/\beta$ is the Fermionic Matsubara frequency, β is the inverse of temperature, ϵ_n is the eigenvalue of $\mathcal{H}_{\rm eff}$, $\eta = -{\rm Im}\Sigma^R$, $\tau = 1/(2\eta)$[40], $\epsilon_{nm} = \epsilon_n - \epsilon_m$ and $\mathcal{Q}^{\alpha\beta}_{D;n} \equiv \sum_{m\neq n}\mathcal{Q}^{\alpha\beta}_{D;n,m}$ is the dissipative quantum geometric tensor, which correspond to $\langle\partial^\alpha n|\partial^\beta n\rangle$ in the limit of $\eta\to 0$. We call the first term $\sigma^{\alpha;\beta}_M$ as " Matsubara term" because it represents the contribution from the poles of the Fermi distribution functions at the Fermionic Matsubara frequencies. While the contribution from the poles of the advanced Green function σ_G corresponds to the results by the SCB treatment or the RDM method in the limit $\eta\to 0$[41], the Matsubara term σ_M is proportional to η[42] and therefore cannot be condsidered in the SCB treatment or the RDM method. We also note that, in the expression of Eq.(4), the contribution from the poles of the advanced Green function describes the picture of the transport of the quasi-particles with complex energy $\epsilon_n + i\eta$ and the variable of the Fermi DF changes to a complex number, while the Fermi-Dirac statistics of electrons are kept since their operators satisfies the anti-commutation relations. Next, we analyze the second term in Eq. (4). We can understand the dissipative geometric term as the multi-band correction to the Drude term, which reads,

$$\tilde{\sigma}^{\alpha\beta}_{\rm Drude} = \sigma^{\alpha\beta}_{\rm Drude} + \sigma^{\alpha\beta}_{\rm QM:re} \tag{6}$$

$$\sigma^{\alpha\beta}_{\rm QM:re} \sim \sum_{\boldsymbol{k}}\sum_{n}\frac{g^{\alpha\beta}_{S;n}}{\tau}\Big(-\frac{\partial f}{\partial\omega}\Big)_{\epsilon_n} \tag{7}$$

$$g^{\alpha\beta}_{S;n} = \sum_m g^{\alpha\beta}_{S;n,m},\quad g^{\alpha\beta}_{S;n,m} = \frac{(\mathcal{J}^{\alpha}_{nm}\mathcal{J}^{\beta}_{mn}+\mathcal{J}^{\beta}_{nm}\mathcal{J}^{\alpha}_{mn})}{2(\epsilon^2_{nm}+4\eta^2)}. \tag{8}$$

The detail derivation is written in appendix A. We can derive $\sigma^{\alpha\beta}_{\rm QM:re}$ from the dissipative geometric term. We call $g^{\alpha\beta}_{S;n}$ as the "smeared quantum metric," which becomes the quantum metric in $\eta\to 0$ limit, and $\sigma^{\alpha\beta}_{\rm QM:re}$ as the "(smeared) quantum metric term". At the band degeneracy where $\epsilon_{nm}=0$, the smeared quantum metric is proportional to τ^2, and therefore, the quantum metric term becomes proportional to τ. We note that this quantum metric correction was pointed out in two-band models in Ref.[43]. This means the quantum metric term describes the multi-band correction to the Drude term, which is proportional to τ. We note that we can also derive this correction from the reduced density matrix methods under the RTA, by changing $f(\epsilon_n)\to f(\epsilon_n+i\eta)$ and approximating ${\rm Im}f(\epsilon_n+i\eta)\simeq\eta(\partial f/\partial\omega)_{\epsilon_n}$. Therefore, we can consider that the quantum metric term stems from the imaginary part of the Fermi DF. We also numerically check how large these terms are and show that the quantum metric term is dominant when the band degeneracy exists at the Fermi surface in appendix C. We also show in appendix C that the Matsubara term is also finite, and therefore, the treatment in this section is not so effective in linear response cases. On the other hand, as we will show in the next section, the Matsubara term is small, and the description by the shift of the Fermi DF to the imaginary direction works well in the nonlinear responses.

III. DISSIPATION-INDUCED GEOMETRY IN NONLINEAR RESPONSE

A. formulation

Next, we consider the effect of the broadening of DF on second-order nonlinear DC conductivity by the same procedure as the linear case. In nonlinear conductivity, many terms emerge from the dissipation effect, and the formula becomes so complicated. Therefore, we write the detailed derivation in appendix D, and here write down the final and summarized results, which read,

$$\sigma^{\alpha;\beta\gamma}_{\rm DC} = \sigma^{\alpha;\beta\gamma}_{\rm M} + \sigma^{\alpha;\beta\gamma}_{\rm G} \tag{9}$$

$$\sigma^{\alpha;\beta\gamma}_{\rm G} = \sigma^{\alpha;\beta\gamma}_{\rm Drude} + \sigma^{\alpha;\beta\gamma}_{\rm BCD} + \sigma^{\alpha;\beta\gamma}_{\rm ChS} + \sigma^{\alpha;\beta\gamma}_{\rm gBC} + \mathcal{O}(\tau^{-2}). \tag{10}$$

$\sigma^{\alpha;\beta\gamma}_{\rm M}$, $\sigma^{\alpha;\beta\gamma}_{\rm G}$, $\sigma^{\alpha;\beta\gamma}_{\rm Drude}$, $\sigma^{\alpha;\beta\gamma}_{\rm BCD}$, $\sigma^{\alpha;\beta\gamma}_{\rm ChS}$, and $\sigma^{\alpha;\beta\gamma}_{\rm gBC}$ represent respectively the Matsubara term in nonlinear conductivity, the sum of the contribution from the poles of the advanced Green function the nonlinear Drude term, the Berry curvature dipole (BCD) term, the Christoffel symbol term, and the generalized Berry curvature term. Here, we newly elucidate last two terms, $\sigma^{\alpha;\beta\gamma}_{\rm ChS}$ and 1 $\sigma^{\alpha;\beta\gamma}_{\rm gBC}$, by considering the effect of dissipation. It is known that the terms including G^A are proportional to $\partial f/\partial\omega$ (see Eq.(16) in Ref.[36]), and therefore, we can divide σ into σ_G, which includes only the Fermi surface term, and σ_M, the contribution from the Matsubara poles. In $\eta\to 0$, σ_G correspond to the Fermi surface term

in Eq.(E5) in Ref.[36] except for the Christoffel symbol term, and σ_M must be zero because it is proportional to η. This means that the Fermi sea term must be zero in $\eta \to 0$ and in the DC limit. Under $\mathcal{T}$-symmetry, $\sigma_{\rm Drude}$ and $\sigma_{\rm ChS}$ must be zero, while under $\mathcal{PT}$-symmetry, $\sigma_{\rm BCD}$ and $\sigma_{\rm gBC}$ must be zero. We summarize τ-dependence of the dominant contribution of each term in Table I. Below, we describe the detailed analysis of each term.

TABLE I. Symmetry classification and τ-dependence

term	$\mathcal{T}$	$\mathcal{PT}$	τ-dependence
$\sigma_{\rm M}$	-	-	$\mathcal{O}(\tau^{-1})$
$\sigma_{\rm Drude}$	$\times$	✓	$\mathcal{O}(\tau^{2})$
$\sigma_{\rm BCD}$	✓	$\times$	$\mathcal{O}(\tau)$
$\sigma_{\rm ChS}$	$\times$	✓	$\mathcal{O}(\tau^{0})$ $(\mathcal{O}(\tau^{2}))$
$\sigma_{\rm gBC}$	✓	$\times$	$\mathcal{O}(\tau^{-1})$

B. analysis of each term

In this subsection, we analyze each term in Eq. (10). Each term, except for the Matsubara term, is so complex, and therefore, we write the simple forms under some approximations, which are $\mathrm{Im}f(\epsilon_n + i\eta) \simeq \eta(\partial f/\partial\omega)_{\epsilon_n}$ and $\epsilon_{nm}^2\tau^2 \gg 1$. We write the detail derivation of each term and the full terms without approximation in appendix D. We also note that the approximation $\mathrm{Im}f(\epsilon_n + i\eta) \simeq \eta(\partial f/\partial\omega)_{\epsilon_n}$ can be justified even when $\beta\eta \sim 0.5$.(see appendix A.)

1. Matsubara term in nonlinear conductivity

The Matsubara term in nonlinear conductivity is the contribution from the poles at Fermionic Matsubara frequencies as in the case of linear conductivity:

$$\begin{aligned}\sigma_{\rm M}^{\alpha;\beta\gamma} &= \sum_{nml}\sum_{\omega_M>0}\mathrm{Re}\Big[\frac{\partial}{\partial\omega}\Big\{2\mathcal{J}^{\alpha}_{nm}\frac{\partial G^R_m}{\partial\omega}\mathcal{J}^{\beta}_{ml}G^R_l\mathcal{J}^{\gamma}_{ln}(G^R_n-G^A_n)\\ &\quad+\mathcal{J}^{\alpha}_{nm}\frac{\partial G^R_m}{\partial\omega}\mathcal{J}^{\beta\gamma}_{mn}(G^R_n-G^A_n)\Big\}+\Big\{\beta\leftrightarrow\gamma\Big\}\Big]_{\omega=i\omega_M},\end{aligned} \tag{11}$$

where $\mathcal{J}^{\beta\gamma} = \partial^{\beta\gamma}\mathcal{H}_{\rm eff}$ and $\partial^{\beta\gamma} = \partial^{\beta}\partial^{\gamma}$. As we will numerically show, in the second-order conductivity under the TRS and the condition $\pi k_B T > \eta$, the Matsubara term is small enough to be ignored, compared with the other finite terms, and therefore, the description by the Fermi DF of complex argument works well.

2. nonlinear Drude term

The nonlinear Drude term can be written as,

$$\sigma^{\alpha;\beta\gamma}_{\rm Drude} \simeq 2\sum_{\boldsymbol{k}}\sum_{n}\tau^2\mathcal{J}^{\alpha}_n\partial^{\beta}\partial^{\gamma}f(\epsilon_n). \tag{12}$$

Because the nonlinear Drude term is proportional to τ^2, this term is most dominant in clean metals without TRS. We note that, if there is the band degeneracy at the Fermi surface, the Christoffel symbol term can be also dominant as we will show later.

3. Berry curvature dipole term

The BCD term[7, 44] can be written as,

$$\sigma^{\alpha;\beta\gamma}_{\rm BCD} = \sigma^{\alpha;\beta\gamma}_{\rm BCD:re} + \sigma^{\alpha;\beta\gamma}_{\rm BCD:im} \tag{13}$$

$$\sigma^{\alpha;\beta\gamma}_{\rm BCD:re} \simeq 2\tau\sum_{\boldsymbol{k}}\sum_{nm}\partial^{\gamma}(\Omega^{\alpha\beta}_{S;n,m})f(\epsilon_n) \tag{14}$$

$$\sigma^{\alpha;\beta\gamma}_{\rm BCD:im} \simeq \sum_{\boldsymbol{k}}\sum_{nm}\frac{\Omega^{\alpha\beta}_{S;n}\mathcal{J}^{\gamma}_n}{\epsilon_{nm}\tau}\Big(\frac{\partial^2 f}{\partial\omega^2}\Big)_{\epsilon_n} \tag{15}$$

$$\Omega^{\alpha\beta}_{S;n,m} = \frac{-i(\mathcal{J}^{\alpha}_{nm}\mathcal{J}^{\beta}_{mn}-\mathcal{J}^{\beta}_{nm}\mathcal{J}^{\alpha}_{mn})}{\epsilon^2_{nm}+4\eta^2} \tag{16}$$

Under the TRS, the nonlinear Drude term must be zero, and the BCD term is dominant. Because $\sigma^{\alpha;\beta\gamma}_{\rm BCD:im}$, which stems from the imaginary part of the Fermi DF, is proportional to η, it is not so large in clean systems. Here we can describe the BCD term by the smeared Berry curvature $\Omega^{\alpha\beta}_{S;n}$, which secures the convergence of the BCD term at the band-crossing points.

4. Christoffel symbol term

The Christoffel symbol term can be described as,

$$\sigma^{\alpha;\beta\gamma}_{\rm ChS} = \sigma^{\alpha;\beta\gamma}_{\rm ChS:I} + \sigma^{\alpha;\beta\gamma}_{\rm ChS:II} \tag{17}$$

$$\sigma^{\alpha;\beta\gamma}_{\rm ChS:I} = 2\sum_{\boldsymbol{k}}\sum_{n}\Gamma^{\alpha;\beta\gamma}_{S;n}\Big(-\frac{\partial f}{\partial\omega}\Big)_{\epsilon_n} \tag{18}$$

$$\sigma^{\alpha;\beta\gamma}_{\rm ChS:II} \simeq 2\sum_{\boldsymbol{k}}\sum_{n}\Gamma^{\alpha;\beta\gamma}_{S';n}\Big(-\frac{\partial f}{\partial\omega}\Big)_{\epsilon_n} \tag{19}$$

where $\Gamma^{\alpha;\beta\gamma}_{S^{(\prime)};n}$ is the smeared Christoffel symbol of the first kind[37, 45]. Starting from the conventional Christoffel symbol $\Gamma^{\alpha;\beta\gamma}_n$, which reads,

$$\begin{aligned}\Gamma^{\alpha;\beta\gamma}_n &= \frac{1}{2}\Big(\partial^{\gamma}g^{\alpha\beta}_n+\partial^{\beta}g^{\gamma\alpha}_n-\partial^{\alpha}g^{\beta\gamma}_n\Big)\\ &= \frac{1}{2}\Big(\langle\partial^{\alpha}n|\partial^{\beta\gamma}n\rangle+\langle\partial^{\beta\gamma}n|\partial^{\alpha}n\rangle\Big)\end{aligned} \tag{20}$$

$$= \sum_{m(\neq)n}\mathrm{Re}\Big[\frac{\mathcal{J}^{\alpha}_{nm}}{\epsilon^2_{nm}}\Big(\sum_{l(\neq n)}\frac{\mathcal{J}^{\beta}_{ml}\mathcal{J}^{\gamma}_{ln}+(\beta\leftrightarrow\gamma)}{\epsilon_{nl}}+\mathcal{J}^{\beta\gamma}_{mn}\Big)\Big], \tag{21}$$

we define $\Gamma^{\alpha;\beta\gamma}_{S;n}$ by substituing $g^{\alpha\beta}_n \to g^{\alpha\beta}_{S;n}$, and $\Gamma^{\alpha;\beta\gamma}_{S';n}$ by substituting $1/\epsilon_{nl} \to \epsilon_{nl}/(\epsilon^2_{nl}+4\eta^2)$ and $1/\epsilon^2_{nm} \to 1/(\epsilon^2_{nm}+4\eta^2)$. $\sigma^{\alpha;\beta\gamma}_{\mathrm{ChS:I}}$ stems from the imaginary part of the Fermi DF in the term which is originally the BCD terms and the nonlinear Drude term, while $\sigma^{\alpha;\beta\gamma}_{\mathrm{ChS:II}}$ stems from the full interband contribution. Interestingly, in this regime, even though $\sigma^{\alpha;\beta\gamma}_{\mathrm{ChS:I}}$ stems from the imaginary part of the Fermi DF and the dissipation, it seems not to depend the dissipation strength. On the other hand, when we consider the band degeneracy at the Fermi surface $\epsilon_n = \epsilon_m \simeq 0$, the Christoffel symbol term is proportional to τ^2 because $g^{\alpha\beta}_{S;n}$ or $1/(\epsilon^2_{nm}+4\eta^2)$ is proportional to τ^2, and therefore, the Christoffel symbol term also gives the multi-band correction to the nonlinear Drude term. We note that the difference between $\Gamma^{\alpha;\beta\gamma}_{S;n}$ and $\Gamma^{\alpha;\beta\gamma}_{S';n}$ appears when focusing on the band-degeneracy of the two-band systems with linear dispersion. In that case, $\Gamma^{\alpha;\beta\gamma}_{S;n}$ is finite and gives the correction to the nonlinear Drude term while $\Gamma^{\alpha;\beta\gamma}_{S';n}$ is zero. We also note that this Christoffel symbol term is different from the one under magnetic field derived by the SCB treatment.[37]

5. generalized Berry curvature term

The generalized Berry curvature term can be written as,

$$\sigma^{\alpha;\beta\gamma}_{\mathrm{gBC}} = \sigma^{\alpha;\beta\gamma}_{\mathrm{gBC:re}} + \sigma^{\alpha;\beta\gamma}_{\mathrm{gBC:im}} + \sigma^{\alpha;\beta\gamma}_{\mathrm{gBC:add}} \tag{22}$$

$$\sigma^{\alpha;\beta\gamma}_{\mathrm{gBC:re}} \simeq \sum_{\boldsymbol{k}} \sum_{n,m(\neq n)} \frac{\Omega^{\alpha,\beta\gamma}_{S';n,m}}{\epsilon_{nm}\tau}\Big(-\frac{\partial f}{\partial\omega}\Big)_{\epsilon_n} \tag{23}$$

$$\sigma^{\alpha;\beta\gamma}_{\mathrm{gBC:add}} \simeq 2\sum_{\boldsymbol{k}} \sum_{n,m,l(\neq n)} \Big\{\frac{\mathrm{Im}(\mathcal{J}^{\alpha}_{nm}\mathcal{J}^{\beta}_{ml}\mathcal{J}^{\gamma}_{ln})}{\epsilon^2_{nm}\epsilon_{nl}} \times \Big(\frac{1}{\epsilon_{nm}\tau}-\frac{1}{\epsilon_{nl}\tau}\Big)\Big(-\frac{\partial f}{\partial\omega}\Big)_{\epsilon_n} + (\beta\leftrightarrow\gamma)\Big\}, \tag{24}$$

$$\sigma^{\alpha;\beta\gamma}_{\mathrm{gBC:im}} \simeq -\sum_{\boldsymbol{k}}\sum_{n} \frac{\Omega^{\alpha,\beta\gamma}_{S';n}}{\tau}\Big(-\frac{\partial^2 f}{\partial\omega^2}\Big)_{\epsilon_n}, \tag{25}$$

where $\Omega^{\alpha,\beta\gamma}_{S;n}$ is the smeared Berry curvature generalized to the second-order derivative and we define $\Omega^{\alpha;\beta\gamma}_{S';n,m}$ as derived from $\Omega^{\alpha;\beta\gamma}_{n,m}$, which reads,

$$\Omega^{\alpha,\beta\gamma}_{n,m} = 2\mathrm{Im}\Big[\langle\partial^{\alpha}n|m\rangle\langle m|\partial^{\beta\gamma}n\rangle\Big] \tag{26}$$

$$= \sum_{m(\neq)n} \mathrm{Im}\Big[\frac{\mathcal{J}^{\alpha}_{nm}}{\epsilon^2_{nm}}\Big(\sum_{l(\neq n)}\frac{\mathcal{J}^{\beta}_{ml}\mathcal{J}^{\gamma}_{ln}+(\beta\leftrightarrow\gamma)}{\epsilon_{nl}} + \mathcal{J}^{\beta\gamma}_{mn}\Big)\Big], \tag{27}$$

by substituting $1/\epsilon_{nl} \to \epsilon_{nl}/(\epsilon^2_{nl}+4\eta^2)$ and $1/\epsilon^2_{nm} \to 1/(\epsilon^2_{nm}+4\eta^2)$. $\sigma^{\alpha;\beta\gamma}_{\mathrm{gBC:add}}$ is zero when considering the two-band model and therefore it represent the more than two-band correction to $\sigma^{\alpha;\beta\gamma}_{\mathrm{gBC:re}}$. When considering the nonreciprocal transport $\alpha=\beta=\gamma$ under the TRS, only this generalized Berry curvature term can be finite. In that case, the nonreciprocal conductivity is proportional to η, and the dissipation is essential for the nonreciprocal conductivity, as pointed out in Ref.[18]. Moreover, we find that, when we focus on two-band models, higher order terms in momentum, such as k^2 term, in the Hamiltonian is also necessary so that $J^{\alpha\alpha}_{mn} = \langle m|\left(\partial^{\alpha\alpha}\mathcal{H}_{eff}\right)|m\rangle$ is nonzero, for the diagonal part of the finite generalized Berry curvature with $\alpha=\beta=\gamma$. It is because l corresponds to m in Eq. (27) for the two-band model, and hence the diagonal part of the generalized Berry curvature vanishes as $\Omega^{\alpha;\alpha\alpha}_{n,m} = 2\Omega^{\alpha\alpha}_{n,m}\mathcal{J}^{\alpha}/\epsilon_{nm} = 0$.[46] This means that the simple linear Weyl Hamiltonian cannot generate the nonreciprocal transport under the TRS. (see the detail in appendix D.)

C. Model calculation

Now we estimate how large the dissipation-induced geometric terms are in the model calculations. We use the model which effectively describes 2D transition-metal dichalcogenides with uniaxial strain, such as MX_2 (M = Mo, W and X = S, Te)[47–49], which reads,

$$\mathcal{H}_{eff} = \sum_{\boldsymbol{k},s,s'}\Big(\left(\epsilon(\boldsymbol{k})-\mu\right)\sigma^0 + \left(\boldsymbol{h}+\boldsymbol{g}(\boldsymbol{k})\right)\cdot\boldsymbol{\sigma}\Big)_{ss'} c^{\dagger}_{\boldsymbol{k},s}c_{\boldsymbol{k},s'} \tag{28}$$

$$\epsilon(\boldsymbol{k}) = 2t\Big((1-p)\cos(\boldsymbol{k}\cdot\boldsymbol{a_1}) + \cos(\boldsymbol{k}\cdot\boldsymbol{a_2}) + \cos(\boldsymbol{k}\cdot(\boldsymbol{a_1}+\boldsymbol{a_2}))\Big) \tag{29}$$

$$g^x(\boldsymbol{k}) = \frac{\alpha_1}{2}\Big[\sin(\boldsymbol{k}\cdot(\boldsymbol{a_1}+\boldsymbol{a_2})) + \sin(\boldsymbol{k}\cdot\boldsymbol{a_2})\Big] \tag{30}$$

$$g^y(\boldsymbol{k}) = -\frac{\alpha_1}{\sqrt{3}}\Big[\sin(\boldsymbol{k}\cdot\boldsymbol{a_1}) + \frac{\sin(\boldsymbol{k}\cdot(\boldsymbol{a_1}+\boldsymbol{a_2}))-\sin(\boldsymbol{k}\cdot\boldsymbol{a_2})}{2}\Big] \tag{31}$$

$$g^z(\boldsymbol{k}) = \frac{2\alpha_2}{3\sqrt{3}}\Big[\sin(\boldsymbol{k}\cdot\boldsymbol{a_1})+\sin(\boldsymbol{k}\cdot\boldsymbol{a_2})-\sin(\boldsymbol{k}\cdot\boldsymbol{a_1}+\boldsymbol{a_2})\Big], \tag{32}$$

where μ is the chemical potential, $\boldsymbol{h}$ is the magnetic filed, t is the hopping, $\boldsymbol{a_1}=(1,0)$, $\boldsymbol{a_2}=(-0.5,\sqrt{3}/2)$, p represents the effect of the uniaxial strain, and $\alpha_{1(2)}$ is the spin-orbit coupling. When $\boldsymbol{h}=0$, this model holds the TRS, while mirror symmetry of y-direction is broken due to finite p. Because, in this paper, we consider in-plane magnetic field such as $\boldsymbol{h}=(h_x,0,0)$, we can ignore the coupling with the orbital motion. In this section, we set the parameters as $t=0.5, p=0.3, \alpha_1=0.08, \alpha_2=0.06$ in the numerical calculation for Fig. reffig:disp, Fig. 3, 4, and (5. Fig. 2 shows the energy dispersion of the model when $\mu=0$. It has the band degeneracy M-, M'-, and Γ- point and their energy levels are $\epsilon=-0.7$, $\epsilon=-1.3$, $\epsilon=2.7$. The density of states is large near $\epsilon=-1.3$ corresponding to the nearly flat dispersion along K'-M'.

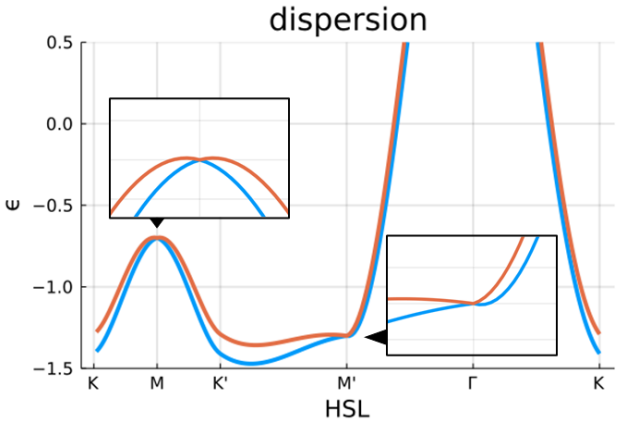

FIG. 2. Dispersion of the model on the high symmetric line. we set $\mu = 0$. The band degeneracy exists at $\epsilon = -0.7$, $\epsilon = -1.3$, and $\epsilon = 2.7$ at M-, M' and Γ-point.

1. *Cases with the time-reversal symmetry*

In this subsection, we calculate the nonlinear Hall conductivity $\sigma^{y;xx}$ and the non-reciprocal conductivity $\sigma^{y;yy}$ in the model introduced above. We note that the model holds the mirror symmetry in x-direction and therefore $\sigma^{x;yy} = \sigma^{y;yx} = \sigma^{x;xx} = 0$. In Fig. 3, we calculate η-dependence, and μ-dependence of the nonlinear Hall conductivity $\sigma^{y;xx}$. Under the time-reversal symmetry, the dominant contribution are the BCD term in Eq. (13) and the generalized Berry curvature (gBC) term in Eq. (22). In the top panel of Fig. 3, as we have shown theoretically, $\sigma_{\mathrm{BCD:re}}$ is proportional to $1/\eta$, while $\sigma_{\mathrm{BCD:im}}$ and σ_{gBC} are proportional to η in the regime $\eta < T$. In the limit $\eta \gg \epsilon_{nm}$, $\sigma_{\mathrm{BCD:im}}$ and σ_{gBC} are proportional to $1/\eta$, and therefore they both decrease in $\eta > 0.04$. At $\eta = \pi T$, due to the singular behavior of $\mathrm{Im}(\partial f/\partial\omega)$, $\sigma_{\mathrm{BCD:im}}$ change its sign and the Matsubara term become large as to compensate it. The bottom panel of Fig. 3 shows μ-dependence. Around $\mu = -1.3$, there is quadratic dispersion at the Fermi surface around at M- and M'-point, and the gBC term becomes large.

Next, we calculate the non-reciprocal conductivity. As I have shown in the previous section, under the time-reversal symmetry, only the gBC term is finite. The top panel of Fig. 4 shows the η-dependence of the non-reciprocal conductivity $\sigma^{y;yy}$. As in the case of the nonlinear Hall conductivity, the gBC term is proportional to η for $\eta < T$ and proportional to $1/\eta$ for $\eta \gg \epsilon_{nm}$.

In the bottom panel of Fig. 4, the non-reciprocal conductivity (gBC term) behaves as same as the gBC term in the nonlinear Hall conductivity. (see the bottome panel of Fig. 3)

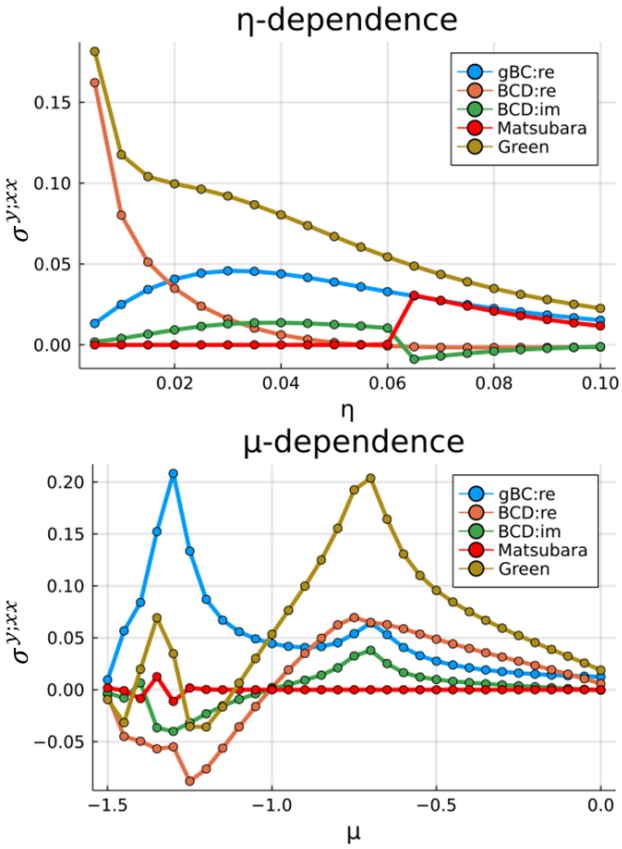

FIG. 3. η-dependence and μ-dependence of each contribution in nonlinear Hall conductivity.
The top panel shows the dissipation-strength dependence of the nonlinear Hall conductivity $\sigma^{y;xx}$, and the bottom panel shows that the chemical potential dependence of $\sigma^{y;xx}$. We set $\mu = -0.9$ in the top panel, $\eta = 0.02$ in the bottom panel, and $k_B T = 0.02$ in both panel. We perform the momentum integration by 1000×1000 and frequency integration by 1000. The blue, orange, green, red, and brown plots respectively represent the generalized Berry curvature term, $\sigma_{\mathrm{BCD:re}}$, $\sigma_{\mathrm{BCD:im}}$, the Matsubara term, and the results by the Green function methods which coincides with the sum of all the terms.

2. *Cases without the time-reversal symmetry*

Next, we consider the case $\boldsymbol{h} \neq 0$, in which time-reversal symmetry is broken. Without the time-reversal symmetry, the Drude term, the Christoffel symbol term can be finite. Here, we focus on the non-reciprocal conductivity with the magnetic field in x-direction $h_x = 0.05$ for Fig. 5.

In time-reversal symmetry broken systems, the (nonlinear) Drude term, which is proportional to τ^2, is dominant in the small dissipation regime. (See the top panel of Fig. 5) The Christoffel symbol term seems also proportional to τ^2 and gives the multi-band correction to the Drude term, because there is band degeneracy around at the Fermi surface.

The bottom panel of Fig. 5 shows the μ-dependence of the non-reciprocal conductivity, In the regime $\mu >$

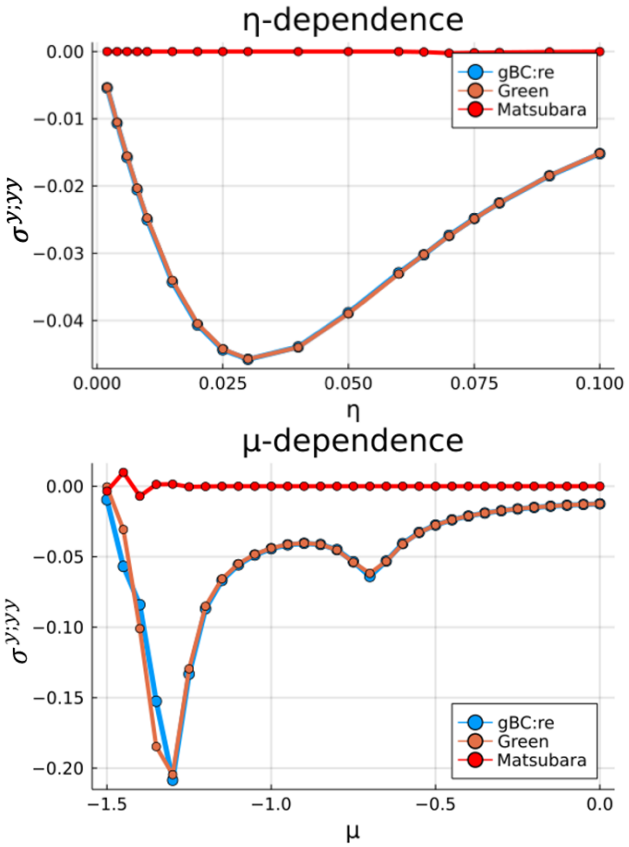

FIG. 4. η-dependence and μ-dependence of each contribution in nonreciprocal conductivity under the time-reversal symmetry.
The top panel shows the dissipation-strength dependence of the non-reciprocal conductivity $\sigma^{y;yy}$, and the bottom panel shows that the chemical potential dependence of $\sigma^{y;yy}$. We set $\mu = -0.9$ in the top panel, $\eta = 0.02$ in the bottom panel, and $k_BT = 0.02$ in both panel. The blue, red, and orange plots respectively represent the generalized Berry curvature term, the Matsubara term, and the results by the Green function methods. We note that blue and orange plots overlap in the upper panel.

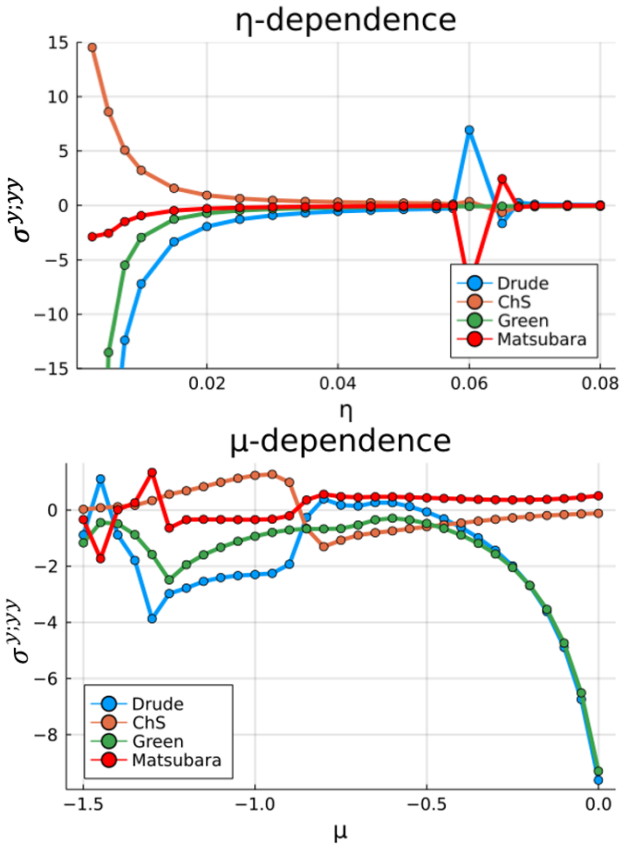

FIG. 5. η-dependence and μ-dependence of each contribution in nonreciprocal conductivity without the time-reversal symmetry.
The top panel shows the dissipation-strength dependence of the non-reciprocal conductivity $\sigma^{y;yy}$, and the bottom panel shows that the chemical potential dependence of $\sigma^{y;yy}$. We set $\mu = -0.9$ in the top panel and $\eta = 0.02$ in the bottom panel, and $k_BT = 0.02$ and $\boldsymbol{h} = (0.05, 0, 0)$ in both panel. The blue, orange, red, and green plots respectively represent the Drude term, the Christoffel symbol term, the Matsubara term, and the results by the Green function methods.

-0.2, the band velocity is large at the Fermi surface, and therefore the Drude term is dominant. On the other hand, in the regime $-0.85 < \mu < -0.5$, the band velocity is not so large and there is the degeneration near the Fermi surface at M'-point, and therefore the Christoffel symbol term is dominant.

IV. NONLINEAR CONDUCTIVITY INDUCED BY DISSIPATIVE QUANTUM GEOMETRY IN THE WEYL HAMILTONIAN

In this section, we derives the analytical results about the geometric terms derived in the previous sections.

A. Hamiltonian and its dissipative quantum geometry

Here, we consider the tilted Weyl Hamiltonian, which reads,

$$\mathcal{H}(\boldsymbol{k}) = (-\mu + \boldsymbol{t}\cdot\boldsymbol{k})\sigma^0 + t_0\boldsymbol{k}\cdot\boldsymbol{\sigma}, \tag{33}$$

where σ^0 is the two by two unit matrix, μ is the chemical potential, t represents the tilting, t_0 is the Fermi velocity, $\boldsymbol{\sigma} = \{\sigma^x, \sigma^y, \sigma^z\}$ is the Pauli matrix. When $t < t_0$, this Hamiltonian describes the type-I Weyl Hamiltonian ,and when $t > t_0$, it describes the type-II Weyl Hamiltonian. Here we set $\boldsymbol{t} = \{0, 0, t\}$ for the simplicity.

In this Hamiltonian, the eigenvalues and the smeared

geometrical quantities are,

$$E_\pm = tk_z \pm t_0 k = t_0 k(\lambda_t \cos\theta \pm 1) \tag{34}$$

$$\mathcal{J}^\alpha_\pm = t_0 k^\alpha(\delta_{\alpha z}\lambda_t \pm 1)/k \tag{35}$$

$$\Omega^{\alpha\beta}_{S;+-} = -\Omega^{\alpha\beta}_{S;-+} = -\Omega^{\beta\alpha}_{S;+-} = \frac{k_\gamma \epsilon_{\alpha\beta\gamma}}{8(k^2+\tilde{\eta}^2)k} \tag{36}$$

$$g^{\alpha\beta}_{S;+-} = g^{\alpha\beta}_{S;-+} = g^{\beta\alpha}_{S;+-} = \frac{\delta_{\alpha\beta}(k^2-k_\alpha^2)}{4(k^2+\tilde{\eta}^2)k^2} \tag{37}$$

where $k = |k|$, $\lambda_t = t/t_0$, $\cos\theta = k_z/k$, and $\tilde{\eta} = \eta/t_0$ is the dissipation strength renormalized by the Fermi velocity. We also define the geometric quantities, which appear in the nonlinear conductivity, as follows:

$$D^{\mu\nu}_\pm \equiv \frac{1}{2}\epsilon^{\mu\lambda\eta}\Omega^{\lambda\eta}_{S;\pm}\mathcal{J}^\nu_\pm = \pm\frac{k_\mu(\delta_{z\nu}\lambda_t \pm k^\nu/k)}{8(k^2+\tilde{\eta}^2)k} \tag{38}$$

$$F^{\mu\nu}_\pm \equiv \partial^\mu g^{\nu\nu}_{S;\pm} = -\frac{k^\mu}{2(k^2+\tilde{\eta}^2)^2k^2}\Big\{(1-\frac{k_\nu^2}{k^2})(2k^2+\tilde{\eta}^2)+\delta_{\mu\nu}(k^2+\tilde{\eta}^2)\Big\} \tag{39}$$

$$\Gamma^{\mu;\nu\eta}_{S;\pm} = \frac{1}{2}(\delta_{\eta\mu}F^{\nu\eta}_\pm + \delta_{\mu\nu}F^{\eta\mu}_\pm - \delta_{\nu\eta}F^{\mu\nu}_\pm) \tag{40}$$

$$\Omega^{\alpha,\beta\gamma}_{S;\pm} = \frac{\pm k(\Omega^{\alpha\beta}_{S;\pm}\mathcal{J}^\gamma_\pm + \Omega^{\alpha\gamma}_{S;\pm}\mathcal{J}^\beta_\pm)}{2(k^2+\tilde{\eta}^2)} \tag{41}$$

In the following, we suppose that $\beta\eta \ll 1$ and the Matsubara term can be ignored. We also approximate $\mathrm{Re}(-\partial f/\partial\omega)_{\epsilon_n+i\eta} \simeq (-\partial f/\partial\omega)_{\epsilon_n} \simeq \delta(\epsilon_n)$ and $\mathrm{Im}f(\epsilon_n+i\eta) \simeq \eta(\partial f/\partial\omega)_{\epsilon_n}$, and then, analyze the geometric terms in the type-I case ($0 < \lambda_t < 1$) and the type-II case ($\lambda_t > 1$) in the regime $\mu \ll \eta$ and $\mu \gg \eta$. We note that, in the former regime, we just focus on the behavior at $\mu \sim 0$.

B. Type-I case

We here consider the case where $\lambda_t < 1$. We can analytically calculate the BCD term and the Christffel symbol term in the limit $\eta \ll |\mu|$ and $\eta \gg |\mu|$ as,

$$\sigma^{\alpha;\beta\gamma}_{\mathrm{BCD;I}} \simeq \tau\int\frac{\boldsymbol{dk}}{(2\pi)^3}\Big\{\Omega^{\alpha\beta}_{S;\pm}\mathcal{J}^\gamma_\pm + (\beta\leftrightarrow\gamma)\Big\}\delta(\epsilon_\pm) \tag{42}$$

$$= \tau\int\frac{\boldsymbol{dk}}{(2\pi)^3}(\delta_{\gamma z}-\delta_{\beta z})\frac{1}{2}\epsilon_{\alpha\beta\gamma}(D^{zz}_\pm) \tag{43}$$

$$= \frac{\tau}{2}\epsilon_{\alpha\beta\gamma}(\delta_{\gamma z}-\delta_{\beta z})\times \tag{44}$$

$$\begin{cases}\frac{1}{8\lambda_t}\Big\{2\lambda_t - \ln\Big(\frac{1+\lambda_t}{1-\lambda_t}\Big)\Big\} & (\eta \ll |\mu|),\\ -\frac{1}{8\lambda_t^3}\frac{\mu^2}{\eta^2}\Big\{2\lambda_t - \tanh^{-1}\Big(\frac{2\lambda_t}{1+\lambda_t^2}\Big)\Big\} & (\eta \gg |\mu|),\end{cases}$$

$$\sigma^{\alpha;\beta\gamma}_{\mathrm{ChS;I}} \simeq \int\frac{\boldsymbol{dk}}{(2\pi)^3}\Gamma^{\alpha;\beta\gamma}_{S;\pm}\delta(\epsilon_\pm) \tag{45}$$

$$= \frac{1}{2}\Big(\delta_{\alpha\beta}\delta_{\gamma z}\tilde{F}^{\gamma\alpha}_{\mathrm{I}} + \delta_{\gamma\alpha}\delta_{\beta z}\tilde{F}^{\beta\gamma}_{\mathrm{I}} - \delta_{\beta\gamma}\delta_{\alpha z}\tilde{F}^{\alpha\beta}_{\mathrm{I}}\Big) \tag{46}$$

with

$$\tilde{F}^{zz}_{\mathrm{I}} = \begin{cases}\frac{\mu}{t_0\lambda_t}\Big\{-\frac{6}{\lambda_t^2}+\frac{3(2-\lambda_t^2)}{2\lambda_t^3}\ln\Big(\frac{1+\lambda_t}{1-\lambda_t}\Big)+\frac{1}{1-\lambda_t^2}\Big\} & (\eta \ll |\mu|),\\ \frac{(3-\lambda_t^2)\mu}{t_0\lambda_t^3}\Big\{\frac{1}{2\lambda_t}\tanh^{-1}\Big(\frac{2\lambda_t}{1+\lambda_t^2}\Big)-\frac{1}{1-\lambda_t^2}\Big\} & (\eta \gg |\mu|),\end{cases} \tag{47}$$

$$\tilde{F}^{zx}_{\mathrm{I}} = \tilde{F}^{zy}_{\mathrm{I}} = \tilde{F}^{xz}_{\mathrm{I}} = \tilde{F}^{yz}_{\mathrm{I}} = \begin{cases}\frac{\mu}{t_0\lambda_t}\Big\{-\frac{6}{\lambda_t^2}+\frac{3(2-\lambda_t^2)}{2\lambda_t^3}\ln\Big(\frac{1+\lambda_t}{1-\lambda_t}\Big)+\frac{1}{1-\lambda_t^2}\Big\} & (\eta \ll |\mu|),\\ \frac{(3-\lambda_t^2)\mu}{t_0\lambda_t^3}\Big\{\frac{1}{2\lambda_t}\tanh^{-1}\Big(\frac{2\lambda_t}{1+\lambda_t^2}\Big)-\frac{1}{1-\lambda_t^2}\Big\} & (\eta \gg |\mu|),\end{cases} \tag{48}$$

Here we omit the analysis of the gBC term, because here we approximate $\mathrm{Re}(-\partial f/\partial\omega)_{\epsilon_n+i\eta} \simeq \delta(\epsilon)$. This approximation is justified when $T \to 0$ and $\eta \to 0$ with $k_B T \gg \eta$, while the gBC term is proportional to η. Interestingly, the nonlinear Hall conductivity by the BCD term is independent of the chemical potential in the regime $|\mu| \gg \eta$, while it is proportional to μ^2/η^2 in the regime $|\mu| \ll \eta$, which results in the dip around $|\mu| < \eta$. The Christoffel symbol term is proportional to μ in both regime. We note that, although Eq. (44) and Eq. (47) appears to diverge at $\lambda_t \to 0$, they becomes zero by appropriately expanding the terms in $\{\dots\}$ in Eq. (44) and Eq. (47).

C. Type-II case

Next, we analyze the type-II Weyl Hamiltonian where $\lambda_t > 1$. Although the only difference in the model from type-I is the magnitude of λ_t, the behavior is completely different. Because the integral of momentum space $\int_0^\infty dk k^2$ is not convergent. Therefore, we introduce the cut-off scale Λ ($\int_0^\infty dk \to \int_0^\Lambda dk$), in which the approximation to the Weyl Hamiltonian is justified. Then, we can derive the BCD term and the Christoffel

symbol term as,

$$\sigma^{\alpha;\beta\gamma}_{\mathrm{BCD;II}} = -\frac{\tau\epsilon_{\alpha\beta\gamma}(\delta_{\gamma z}-\delta_{\beta z})}{32\pi^2\lambda_t}\ln\Big(\frac{\Lambda^2+\eta^2}{(\mu/(1+\lambda_t))^2+\eta^2}\Big) \tag{49}$$

$$\sigma^{\alpha;\beta\gamma}_{\mathrm{ChS;II}} = \frac{1}{2}\Big(\delta_{\alpha\beta}\delta_{\gamma z}\tilde{F}^{\gamma\alpha}_{\mathrm{II}}+\delta_{\gamma\alpha}\delta_{\beta z}\tilde{F}^{\beta\gamma}_{\mathrm{II}}-\delta_{\beta\gamma}\delta_{\alpha z}\tilde{F}^{\alpha\beta}_{\mathrm{II}}\Big) \tag{50}$$

$$\tilde{F}^{zz}_{\mathrm{II}} = \frac{\Lambda}{t_0}\Big(\frac{3}{2\lambda_t^2}-\frac{1}{\lambda_t^4}\Big)+\mathcal{O}(\ln\Lambda) \tag{51}$$

$$\tilde{F}^{zx}_{\mathrm{II}} = \tilde{F}^{zy}_{\mathrm{II}} = \tilde{F}^{xz}_{\mathrm{II}} = \tilde{F}^{yz}_{\mathrm{II}} = \frac{\Lambda}{t_0}\Big(\frac{1}{\lambda_t^2}-\frac{1}{\lambda_t^4}\Big)+\mathcal{O}(\ln\Lambda) \tag{52}$$

In the type-II case, when we consider the limit $\mu \to 0$ with $\eta/\mu = $ const., the BCD term shows a logarithmic divergence, while it is convergence with finite η. This behavior is completely different from the type-I case, where the BCD term has the dip at $\mu = 0$. In the limit $\Lambda \gg t_0, \mu, \eta, \lambda_t$, the dominant term of the Christoffel symbol term is independent of μ and η in the type-II Weyl Hamiltonian.

D. Numerical results

We also check the numerical calculation about the chemical potential dependence of the nonlinear Hall effect $\sigma^{y;zx} = -\sigma^{x;yz}$. Interestingly, in addition to the μ-independence of the nonlinear Hall conductivity at $|\mu| \gg \eta$ as we have analytically shown, the gBC term compensates the dip of the BCD term around $\mu = 0$, which results in complete μ-independence of the nonlinear Hall conductivity.(See the top panel of Fig. 6.) The bottom panel of Fig. 6 shows that the peak behaviour of the nonlinear Hall conductivity at $\mu = 0$ as we have shown, and its order of the conductivity is much larger than type-I Weyl systems. This result means that the type-II Weyl materials can show large nonlinear Hall effect.

We again stress that this chemical potential independence or the peak behavior of the nonlinear Hall conductivity can be highly utilized for the detection of the Weyl points and their type.

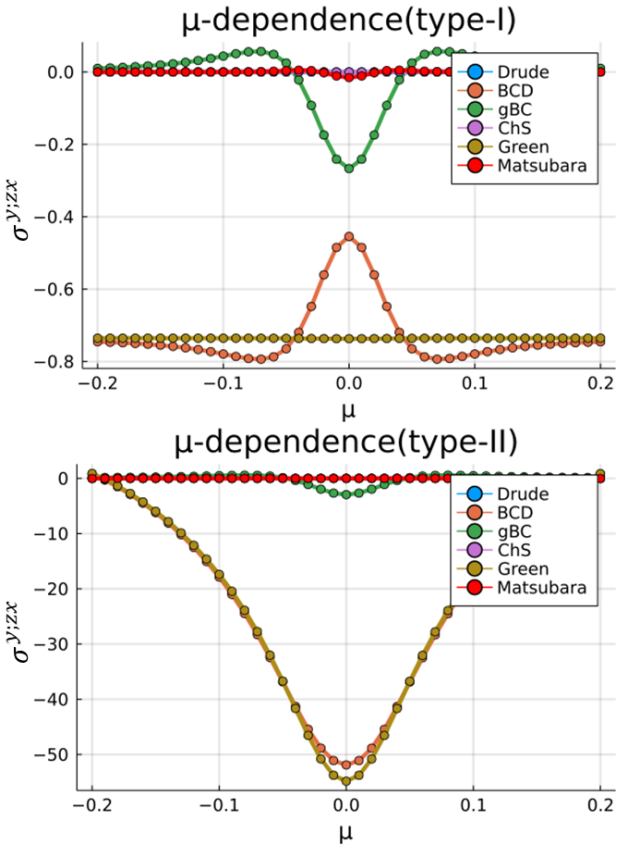

FIG. 6. μ-dependence of the nonlinear Hall conductivity in type-I and II Weyl Hamiltonian.
The top (bottom) panel shows the nonlinear Hall conductivity in the type-I (II) Weyl Hamiltonian. We set the parameter as $t_0 = 1.0, t = 0.3$ for the type-I Weyl Hamiltonian and $t_0 = 0.3, t = 0.5$ for the type-II Weyl Hamiltonian. We also set $k_BT = 0.02$ and $\eta = 0.01$ for each case. The terms except the BCD term and the gBC term are almost zero.

V. SUMMARY AND OUTLOOK

In this paper, we have analyzed the dissipation effect on the linear and nonlinear DC conductivity under the Markov approximation in multi-band systems.

Starting from the Green function formalism, we elucidate the effect of the dissipation: the shift of the distribution function in the imaginary direction and the Matsubara term, which cannot be included by the conventional methods such as the SCB treatment and the reduced density matrix methods. Moreover, we clarify that the novel terms from the imaginary part of the distribution function also have a geometric nature, such as the quantum metric term in the linear conductivity, the Christoffel symbol term, and the generalized Berry curvature term in the nonlinear conductivity. These terms give the multi-band correction to the (nonlinear) Drude term when there is band degeneracy at the Fermi surface. Although the Matsubara term is not small in the linear response, it is small enough to be ignored in the nonlinear conductivities, especially under the TRS, and therefore, the description of the Fermi DF of complex argument works well. Under the TRS, the inversion symmetry breaking is encoded in the multi-band effect such as the BCD and the generalized Berry curvature. At the pole of the Matsubara frequency, the large imaginary value of $i\omega_M$ in the denominator of the $G(i\omega_M)$ cloaks such kind of geometric structure, and therefore, the Matsubara term becomes almost zero. When $\pi k_BT \sim \eta$, $i\omega_M - i\eta$ in the denominator of $G^A(i\omega_M)$ becomes almost zero, and the above cloaking is unveiled, and the Matsubara term becomes finite. In the nonlinear conductivity without TRS and the linear conductivity, the

Drude term, which is the intra-band contribution and does not need the geometric structure, can be finite, and therefore, the Matsubara term can also be finite.

We have also elucidated the geometric origin of the non-reciprocal conductivity under the TRS, which can be described by the Berry curvature generalized to the higher-order derivative. For two-band systems, we have identified another condition of the non-reciprocal conductivity under the time-reversal symmetry, that is, the quadratic term, in addition to the dissipation which is pointed out in Ref.[18].

Then, we numerically calculate the η- and μ-dependence of each contribution in the model which describes TMD materials. The results show that the Matsubara term becomes large at $\eta > \pi k_B T$ when the terms from the imaginary part of the distribution function are not small. We have shown that, in some regime, the novel geometric term become dominant.

Finally, we analyze each geometric term in the Weyl Hamiltonian. We clarify that the chemical potential dependence around the Weyl point of nonlinear Hall conductivity is completely different between the type-I and type-II case. While the nonlinear Hall conductivity is independent of the chemical potential in the type-I case, it shows the logarithmic divergence behavior at the energy level where the Weyl points exist in the type-II case. This result suggests that detecting the chemical potential dependence of the nonlinear Hall conductivity under the time-reversal symmetry can be utilized to detect the existence of the Weyl points and their type. Moreover, we also show that the type-II Weyl materials can show large nonlinear Hall conductivity due to their divergent behavior at the Weyl points.

Although we consider the DC conductivity in this paper, a similar analysis can be applied to the photovoltaic effect, in which dissipation holds an important role. It is left for future work.

ACKNOWLEDGE

YM deeply appreciate to Hikaru Watanabe, Yoichi Yanase, and Kazuaki Takasan for fruitful discussions. YM also thanks Masahiko G. Yamada, Atsuo Shitade, and Hiroshi Shinaoka for their advice about the numerical calculations. We performed all calculation with Julia[50]. The code which we used is uploaded to https://github.com/YoshihiroMichishita/julia. This work was partially supported by WISE program, MEXT. YM was supported by a JSPS research fellowship and by JSPS KAKENHI (Grant No. 20J12265), and is supported by RIKEN SPDR. Naoto Nagaosa is supported by JSPS KAKENHI Grant (No. 18H03676), and by JST CREST Grant Number JPMJCR1874, Japan.

Note added. – While revising the manuscript, we noticed a related paper by Daniel Kaplan, Tobias Holder, and Binghai Yan.[51] They analyze the dissipation effect on nonlinear conductivity by first calculating in $\tau \to \infty$ limit and then restoring the finite τ, which results in ignoring the essential part of the generalized Berry curvature term in Eq.(22). For an example, their τ^{-1} dependent term must disappear in longitudinal nonreciprocal conductivity, while our generalized Berry curvature term can be finite.

Appendix A: Detail derivation of the dissipation-induced geometric term in linear conductivity

Contribution from the pole of the advanced Green functions to the linear conductivity can be described as follows,

$$\sigma^{\alpha\beta}_{\rm G} = \sigma^{\alpha\beta}_{\rm Drude} + \sigma^{\alpha\beta}_{\rm QM:re} + \sigma^{\alpha\beta}_{\rm QM:im} \tag{A1}$$

$$\sigma^{\alpha\beta}_{\rm Drude} = \sum_{\boldsymbol{k}} \sum_{n} \mathcal{J}^{\alpha}_{n} \mathcal{J}^{\beta}_{n} \tau {\rm Re}\Big(-\frac{\partial f}{\partial \omega}\Big)_{\epsilon_n + i\eta} \tag{A2}$$

$$\sigma^{\alpha\beta}_{\rm QM:re} = \sum_{\boldsymbol{k}} \sum_{n} \frac{g^{\alpha\beta}_{S;n}}{\tau} {\rm Re}\Big(-\frac{\partial f}{\partial \omega}\Big)_{\epsilon_n + i\eta} \tag{A3}$$

$$\sigma^{\alpha\beta}_{\rm QM:im} = \sum_{\boldsymbol{k}} \sum_{n} \sum_{m\neq n} g^{\alpha\beta}_{S;n,m} \epsilon_{nm} {\rm Im}\Big(-\frac{\partial f}{\partial \omega}\Big)|_{\epsilon_n + i\eta} \tag{A4}$$

$$g^{\alpha\beta}_{S;n,m} = \frac{(\mathcal{J}^{\alpha}_{nm}\mathcal{J}^{\beta}_{mn} + \mathcal{J}^{\beta}_{nm}\mathcal{J}^{\alpha}_{mn})}{2(\epsilon^2_{nm} + 4\eta^2)}. \tag{A5}$$

We call $g^{\alpha\beta}_{S;n}$ as "the smeared quantum metric." We note that the smeared geometric quantities are well defined and finite at gapless points where $\epsilon_{nm} = 0$. $\sigma^{\alpha\beta}_{\rm QM:re} + \sigma^{\alpha\beta}_{\rm QM:im}$ is the novel term, which we call "quantum metric term" at the Fermi surface.

We note that we can approximate ${\rm Re}f(\epsilon_n + i\eta) \simeq f(\epsilon_n)$ and ${\rm Im}f(\epsilon_n + i\eta) \simeq \eta \partial f(\epsilon_n)/\partial\omega$ when $\beta\eta \ll 1$. Fig. 7 shows that this approximation is valid even when $\beta\eta \sim 0.5$. Under this approximation, in the both limits $\epsilon_{nm} \gg \eta$ and $\epsilon_{nm} \to 0$, the terms proportional to the imaginary part of the distribution function can be written as,

$$g^{\alpha\beta}_{S;n,m} \epsilon_{nm} {\rm Im}\Big(-\frac{\partial f}{\partial \omega}\Big)|_{\epsilon_n + i\eta} \simeq \frac{\epsilon_{nm}}{2\tau} g^{\alpha\beta}_{S;n,m} \Big(-\frac{\partial^2 f}{\partial \omega^2}\Big)|_{\epsilon_n} \tag{A6}$$

When we see the frequency derivative of the Fermi distribution function as $\sim \mathcal{O}(\beta)$, the imaginary part contributions are the order $\sim \mathcal{O}(\epsilon_{nm}\beta)$ compared to the real part of the contribution. This means that the contribution from the imaginary part of the distribution function can be dominant at low temperature. We note that, under the approximation ${\rm Re}f(\epsilon_n + i\eta) \simeq f(\epsilon_n)$ and ${\rm Im}f(\epsilon_n + i\eta) \simeq \eta \partial f(\epsilon_n)/\partial\omega$, Eq. (A3) can be derived from the RDM methods by substituting $f(\epsilon_n) \to f(\epsilon_n + i\eta)$ in the anomalous quantum Hall term and considering the imaginary part of the Fermi distribution function. From this point of view, $\sigma^{\alpha\beta}_{\rm QM:re}$ also originates from the imaginary part of the distribution function in the anomalous quantum Hall term.

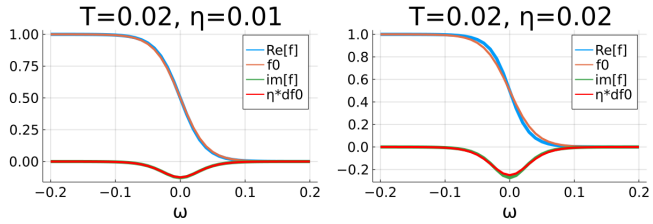

FIG. 7. Approximation about the imaginary part of the distribution function.
The blue(orange) plots show the real(imaginary) part of $f(\omega+i\eta)$. The green plots show $f(\omega)$ and the red plots show $\eta\partial f/\partial\omega$. The parameters are $T=0.02$, and $\eta=0.01$ on the left panel and $\eta=0.02$ on the right panel. This figure shows that the approximation $\mathrm{Re}f(\omega+i\eta)\simeq f(\omega)$ and $\mathrm{Im}f(\omega+i\eta)\simeq\eta\partial f(\omega)/\partial\omega$ is enough good even when $\beta\eta\sim 0.5$.

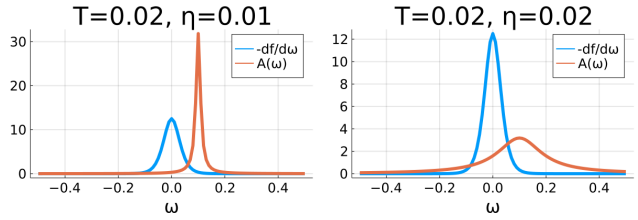

FIG. 8. broadening of the spectral function v.s. derivative of the Fermi DF.
The blue(orange) plots show the ω-derivative of the Fermi DF $(-\partial f/\partial\omega)$ (the spectral function $A(\omega)$). Here we set the temperature $T=0.02$, and $\epsilon_n=0.1$. $\eta=0.01(0.1)$ in the left(right) panel.

When considering the band degeneracy at the Fermi surface, which means $\epsilon_n=\epsilon_m$, the smeared quantum metric $g^{\alpha\beta}_{S;n}$ is proportional to τ^2 and the quantum metric term in Eq. (A3) is proportional to τ, which means the quantum metric term gives the multi-band correction to the Drude term in Eq. (A2). Therefore, the quantum metric term becomes important in materials with large band degeneracy at the Fermi surface or the strongly-dissipative system.

Appendix B: Intuitive understanding about the Matsubara term

In this part, we give an intuitive understanding of the shift of the Fermi DF and the Matsubara term. In the conventional band representation, the occupancy of the band is determined by its energy and the Fermi DF $(f(\epsilon_n))$, and it is true in the limit of $\eta\to 0$. However, when η is finite, there is a broadening of the spectral function, and the occupancy of the band cannot be determined just by the band energy and the Fermi DF. In the small dissipation regime $\eta\ll T$, the broadening is small, and the bands with the energy level where $(df/d\omega)_{\epsilon_n}$ is finite contribute to the transport. For example, in Fig. 8, the band, whose energy is $|\epsilon_n|>T$, almost does not contribute to the transport. In this case, the description by the Fermi DF is accurate, and the shift of the Fermi DF to the imaginary direction well approximates the broadening of the spectral function. On the other hand, when we consider the highly dissipative case $\eta>T$, even though the band energy is far away from the Fermi energy $|\epsilon_n|\gg T$ and $(df/d\omega)_{\epsilon_n}\simeq 0$, there is the overlap between $df(\omega)/d\omega$ and $A(\omega)$, and this band can contribute to the transport. In this case, the description by the Fermi DF becomes bad, and the Matsubara term, which is not described by the Fermi DF, can become large. This understanding should also hold in nonlinear conductivity.

Appendix C: model calculation

We numerically calculate these contribution to the linear conductivity in the nodal-line semimetals, which is described by the following Hamiltonian as[52],

$$\mathcal{H}=\mu\tau^0+t(2+\cos k_0-\cos k_x-\cos k_y-\cos k_z)\tau^z +v\sin k_z\tau^y+\Delta\tau^x. \tag{C1}$$

μ,t,v,Δ represent the chemical potential, the hopping amplitude, the hybridization, and the TRS breaking parameter. We note that this tight-binding Hamiltonian describes the low-energy dispersion near the Fermi level of CaAgP and Ca_3P_2[53, 54]. For the upper panel of Fig. 9, the chemical potential (μ) dependence of the linear conductivity is shown. Here the temperature $k_BT=0.02$, $\eta=0.04$, and $\Delta=0$. This model has the nodal line at the Fermi surface when $\mu=0,\Delta=0$ and the quantum metric term becomes large. We note that, in this model, $\mathcal{J}^z_{nn}$ is zero on the nodal line and therefore the Drude term becomes almost zero at $\mu=0$, while the qunatum metric term and the Matsubara term are finite due to the broadening of the spectral weight and the hybridization.

In this case, the quantum metric term and the Matsubara term cannot be ignored for finite *eta*, and the Matsubara term is dominant when $\eta>\pi T$. Even when the system has a quadratic band touching at the Fermi surface and the Drude term is zero, if these bands are constructed by the hybridization, the linear conductivity can be finite due to the quantum metric term.

The bottom panel of Fig. 9 shows that η-dependence of the linear conductivity. Here the temperature $T=0.02$, $\mu=0$, and $\Delta=0$. In the small dissipation regime, the quantum metric term and the Matsubara term are proportional to η, and therefore, the Drude term is dominant. In our formulation, $\eta=\pi T$, where the Fermi distribution function $f(\epsilon_n+i\eta)$ behaves as the Bose distribution function $f_B(\epsilon_n)$, is a singular. In the large dissipation regime where $\eta>\pi T$, the contribution from the Drude term becomes almost zero. This large dissipation regime at low temperature can be realized in the quantum critical regime because the large quantum fluctuation behaves as the large dissipation from the single-

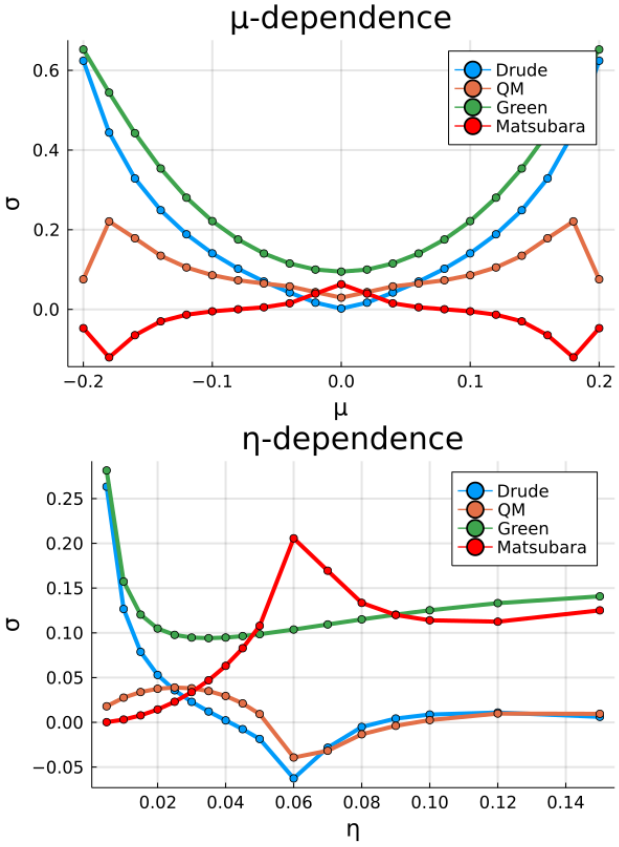

FIG. 9. Linear conductivity in a nodal-line semimetal. The parameters are $T = 0.02, \eta = 0.04$ on the top panel and $T = 0.02, \mu = 0$ on the bottom panel. We perform the momentum integration by $250 \times 250 \times 250$ and frequency integration by 1000. The blue, orange, green, red plots respectively describe the Drude term, the quantum metric term $(\sigma^{zz}_{\mathrm{QM:re}} + \sigma^{zz}_{\mathrm{QM:im}})$, the total conductivity calculated by the Green function methods, and the Matsubara term.

particle point of view. In such a regime, the SCB treatment and the reduced density matrix method are not appropriate, and we must use the Green function methods.

The relaxation time τ in usual materials is about $1 \sim 100$ picosecond[27], which equals to $\eta \simeq 2.1 * 10^{-5} \sim 2.1 * 10^{-3}$[eV]. In this case, the temperature which satisfies $\pi k_B T > \eta$ is about $T > 7.5 * 10^{-2} \sim 7.5$[K], and this condition is often not satisfied in the condensed matter physics. Therefore, our result shows that we should consider the broadening of the spectral function or, to say, the quantum dissipation at low temperature, and the SCB treatment or the reduced density matrix formalism is not appropriate, especially when we consider the transport at a degenerated Fermi surface.

Appendix D: Detail derivation of the dissipation-induced geometric terms in nonlinear conductivity

The nonlinear conductivity is described with the Green function formalism as

$$\sigma^{\alpha;\beta\gamma}_{\mathrm{DC}} = \int_{-\infty}^{\infty} \frac{d\omega}{2\pi} \mathrm{ImTr}\Big[\Big\{2\mathcal{J}^{\alpha}_{nm}\frac{\partial G^R_m}{\partial\omega}\mathcal{J}^{\beta}_{ml}G^R_l\mathcal{J}^{\gamma}_{ln}(G^R_n - G^A_n) + \mathcal{J}^{\alpha}_{nm}\frac{\partial G^R_m}{\partial\omega}\mathcal{J}^{\beta\gamma}_{mn}(G^R_n - G^A_n)\Big\} + \{\beta \leftrightarrow \gamma\}\Big], \tag{D1}$$

where $\mathcal{J}^{\beta\gamma} = \partial^{\beta}\partial^{\gamma}\mathcal{H}_{\mathrm{eff}}$. By starting from this Green function formalism and performing the same procedure as in the linear case, we can derive the following equation as,

$$\sigma^{\alpha;\beta\gamma}_{\mathrm{DC}} = \sum_{\boldsymbol{k}}\Big(\sigma^{\alpha;\beta\gamma}_{\mathrm{M}} + \tilde{\sigma}^{\alpha;\beta\gamma}_{\mathrm{Drude}} + \tilde{\sigma}^{\alpha;\beta\gamma}_{\mathrm{BCD}} + +\tilde{\sigma}^{\alpha;\beta\gamma}_{\mathrm{Inter}}\Big), \tag{D2}$$

$$\sigma^{\alpha;\beta\gamma}_{\mathrm{Th}} = \sum_{nml}\sum_{\omega_M>0}\mathrm{Re}\Big[\frac{\partial}{\partial\omega}\Big\{2\mathcal{J}^{\alpha}_{nm}\frac{\partial G^R_m}{\partial\omega}\mathcal{J}^{\beta}_{ml}G^R_l\mathcal{J}^{\gamma}_{ln}(G^R_n - G^A_n) + \mathcal{J}^{\alpha}_{nm}\frac{\partial G^R_m}{\partial\omega}\mathcal{J}^{\beta\gamma}_{mn}(G^R_n - G^A_n)\Big\} + \Big\{\beta \leftrightarrow \gamma\Big\}\Big]_{\omega=i\omega_M} \tag{D3}$$

$$\tilde{\sigma}^{\alpha;\beta\gamma}_{\mathrm{Drude}} = 2\sum_{n}\tau^2\mathrm{Re}\Big[\mathcal{J}^{\alpha}_n\mathcal{J}^{\beta}_n\mathcal{J}^{\gamma}_n\Big(-\frac{\partial^2 f}{\partial\omega^2}\Big) + \mathcal{J}^{\alpha}_n\mathcal{J}^{\beta\gamma}_n\Big(-\frac{\partial f}{\partial\omega}\Big) + \sum_{m(\neq n)}\mathcal{J}^{\alpha}_n\frac{\mathcal{J}^{\beta}_{nm}\mathcal{J}^{\gamma}_{mn} + (\beta \leftrightarrow \gamma)}{\epsilon_{nm} + 2i\eta}\Big(-\frac{\partial f}{\partial\omega}\Big)\Big]_{\omega=\epsilon_n+i\eta} \tag{D4}$$

$$\tilde{\sigma}^{\alpha;\beta\gamma}_{\mathrm{BCD}} = 2\sum_{n}\tau\mathrm{Im}\Big[\mathcal{Q}^{\alpha\beta}_{D;n}\mathcal{J}^{\gamma}_n\Big(-\frac{\partial f}{\partial\omega}\Big) + (\beta \leftrightarrow \gamma)\Big]_{\omega=\epsilon_n+i\eta} \tag{D5}$$

$$\tilde{\sigma}^{\alpha;\beta\gamma}_{\mathrm{Inter}} = 2\sum_{nm(m\neq n)}\mathrm{Re}\Big[\frac{\mathcal{J}^{\alpha}_{nm}\mathcal{J}^{\beta\gamma}_{mn}}{(\epsilon_{nm} + 2i\eta)^2}\Big(-\frac{\partial f}{\partial\omega}\Big) + \sum_{l\neq n}\frac{\mathcal{J}^{\alpha}_{nm}\mathcal{J}^{\beta}_{ml}\mathcal{J}^{\gamma}_{ln} + (\beta \leftrightarrow \gamma)}{(\epsilon_{nm}+2i\eta)^2(\epsilon_{nl}+2i\eta)}\Big(-\frac{\partial f}{\partial\omega}\Big)\Big]_{\omega=\epsilon_n+i\eta} \tag{D6}$$

$\sigma^{\alpha;\beta\gamma}_{\mathrm{M}}$ is the Matsubara term for the second order nonlinear response. Tilde above the terms means the classification of terms in the limit $\eta \to 0$. First, we analyze the "Drude term" $\tilde{\sigma}^{\alpha;\beta\gamma}_{\mathrm{Drude}}$, which corresponds to the Drude term in the conventional analysis. While the first term and second term in Eq. (D4) only get the contri-

bution from the real part of the distribution function, the third term has the contribution from the imaginary part. Under the approximation $\mathrm{Re}f(\epsilon_n+i\eta)\simeq f(\epsilon_n)$ and $\mathrm{Im}f(\epsilon_n+i\eta)\simeq\eta\partial f(\epsilon_n)/\partial\omega$, we can derive the following form from the third term in Eq. (D4) as,

$$\begin{aligned}
&\sum_{m(\neq n)}\mathcal{J}^{\alpha}_{n}\frac{\mathcal{J}^{\beta}_{nm}\mathcal{J}^{\gamma}_{mn}+(\beta\leftrightarrow\gamma)}{\epsilon_{nm}+2i\eta}\Big(-\frac{\partial f}{\partial\omega}\Big)\Big]_{\omega=\epsilon_n+i\eta}\\
&=2\sum_{n\neq m}\tau^2\epsilon_{nm}\mathcal{J}^{\alpha}_{n}g^{\beta\gamma}_{S;n,m}\mathrm{Re}\Big(\frac{\partial f}{\partial\omega}\Big)_{\omega=\epsilon_n+i\eta}\\
&\quad+2\sum_{n}\tau\mathcal{J}^{\alpha}_{n}g^{\beta\gamma}_{S;n}\mathrm{Im}\Big(\frac{\partial f}{\partial\omega}\Big)_{\omega=\epsilon_n+i\eta} \qquad \text{(D7)}\\
&\simeq 2\sum_{n\neq m}\tau^2\epsilon_{nm}\mathcal{J}^{\alpha}_{n}g^{\beta\gamma}_{S;n,m}\Big(\frac{\partial f}{\partial\omega}\Big)_{\omega=\epsilon_n}\\
&\quad+\sum_{n}\mathcal{J}^{\alpha}_{n}g^{\beta\gamma}_{S;n}\Big(\frac{\partial^2 f}{\partial\omega^2}\Big)_{\omega=\epsilon_n} \qquad \text{(D8)}
\end{aligned}$$

The second term newly arise from the imaginary part of the distribution function, which represents the broadening of the spectral function. We note that the other terms in $\tilde{\sigma}_{\mathrm{Drude}}$ can be summarized into the conventional Drude term as $\tau^2\sum_n\mathcal{J}^{\alpha}_{n}\partial^{\beta}\partial^{\gamma}f(\epsilon_n)$ in the limit of $\eta\to 0$. We can transform the second term into

$$\begin{aligned}
\tilde{\sigma}^{\alpha;\beta\gamma}_{\mathrm{Drude}}&=\sigma^{\alpha;\beta\gamma}_{\mathrm{Drude}}+\sigma^{\alpha;\beta\gamma}_{\mathrm{sQMD}} \qquad \text{(D9)}\\
\sigma^{\alpha;\beta\gamma}_{\mathrm{Drude}}&=2\tau^2\sum_{n}\mathcal{J}^{\alpha}_{n}\Big[\mathcal{J}^{\beta}_{n}\mathcal{J}^{\gamma}_{n}\mathrm{Re}\Big(-\frac{\partial^2 f}{\partial\omega^2}\Big)+\\
&\qquad\Big(\mathcal{J}^{\beta\gamma}_{n}+\sum_{m}\epsilon_{nm}g^{\beta\gamma}_{S;n,m}\Big)\Big(-\frac{\partial f}{\partial\omega}\Big)\Big]|_{\epsilon_n+i\eta}\\
&\simeq 2\tau^2\sum_{n}\mathcal{J}^{\alpha}_{n}\partial^{\beta}\partial^{\gamma}f(\epsilon_n) \qquad \text{(D10)}\\
\sigma^{\alpha;\beta\gamma}_{\mathrm{sQMD}}&=2\sum_{n}\tau\mathcal{J}^{\alpha}_{n}g^{\beta\gamma}_{S;n}\mathrm{Im}\Big(\frac{\partial f}{\partial\omega}\Big)_{\omega=\epsilon_n+i\eta}\\
&\simeq\sum_{n}\mathcal{J}^{\alpha}_{n}g^{\beta\gamma}_{S;n}\Big(\frac{\partial^2 f}{\partial\omega^2}\Big)_{\omega=\epsilon_n}\\
&=\sum_{n}\partial^{\alpha}g^{\beta\gamma}_{S;n}\Big(-\frac{\partial f}{\partial\omega}\Big)_{\omega=\epsilon_n}, \qquad \text{(D11)}
\end{aligned}$$

and therefore, we call it the (smeared) quantum metric dipole term. We note that this quantum metric dipole term is different from that in Ref.[55], which needs non-uniform electric fields. Because here it is the smeared quantum metric, when there is a band-degeneracy at the Fermi surface, this term is proportional to τ^2 (because $g^{\beta\gamma}_{S;n}$ is proportional to τ^2 when $\epsilon_{nm}=0$) and gives the multi-band correction to the conventional nonlinear Drude term, as same as the linear conductivity. On the other hand, in the regime $|\epsilon_n-\epsilon_m|\tau\gg 1$, this term becomes almost independent from the strength of the dissipation even though this term stems from the dissipation.

Next, we analyze the originally Berry curvature dipole term. Under the approximation, we can derive

$$\begin{aligned}
\tilde{\sigma}^{\alpha;\beta\gamma}_{\mathrm{BCD}}&=\sigma^{\alpha;\beta\gamma}_{\mathrm{dBCD}}+\sigma^{\alpha;\beta\gamma}_{\mathrm{dQMD}} \qquad \text{(D12)}\\
\sigma^{\alpha;\beta\gamma}_{\mathrm{dBCD}}&=2\sum_{n}\tau\Omega^{\alpha\beta}_{D;n}\mathcal{J}^{\gamma}_{n}\mathrm{Re}\Big(-\frac{\partial f}{\partial\omega}\Big)_{\epsilon_n+i\eta}+(\beta\leftrightarrow\gamma)\\
&=4\tau\sum_{n}\partial^{\gamma}\Omega^{\alpha\beta}_{D;n}\mathrm{Re}f(\epsilon_n+i\eta)+(\beta\leftrightarrow\gamma) \qquad \text{(D13)}\\
\sigma^{\alpha;\beta\gamma}_{\mathrm{dQMD}}&=-2\sum_{n}g^{\alpha\beta}_{D;n}\mathcal{J}^{\gamma}_{n}\mathrm{Im}\Big(-\frac{\partial f}{\partial\omega}\Big)_{\epsilon_n}+(\beta\leftrightarrow\gamma)\\
&=4\tau\sum_{n}\partial^{\gamma}g^{\alpha\beta}_{D;n}\mathrm{Im}f(\epsilon_n+i\eta)+(\beta\leftrightarrow\gamma), \qquad \text{(D14)}
\end{aligned}$$

where $\Omega^{\alpha\beta}_{D;n}=\mathrm{Im}\mathcal{Q}^{\alpha\beta}_{D;n}$ is the dissipative Berry curvature and $\Omega^{\alpha\beta}_{D;n}=2\mathrm{Re}\mathcal{Q}^{\alpha\beta}_{D;n}$ is the dissipative quantum metric. In the limit $\eta\to 0$, Eq. (D13) becomes the well-known the Berry curvature dipole term. We note that the dissipative quantum geometry is different from the smeared quantum geometry. In this representation, because it is the dissipative geometry, the (dissipative) Berry curvature dipole term is not necessarily the Hall conductivity. Therefore, it is more convenient to convert the smeared geometric terms as written as,

$$\begin{aligned}
&\sigma^{\alpha;\beta\gamma}_{\mathrm{dBCD}}\\
&=2\tau\sum_{n,m}\Bigg[\Big(\frac{\epsilon^2_{nm}\tau^2-1}{\epsilon^2_{nm}\tau^2+1}\Omega^{\alpha\beta}_{S;n,m}-\frac{2\epsilon_{nm}\tau}{\epsilon^2_{nm}\tau^2+1}g^{\alpha\beta}_{S;n,m}\Big)\\
&\qquad\times\mathcal{J}^{\gamma}_{n}\mathrm{Re}\Big(-\frac{\partial f}{\partial\omega}\Big)_{\epsilon_n+i\eta}+(\beta\leftrightarrow\gamma)\Bigg] \qquad \text{(D15)}\\
&\simeq 2\tau\sum_{n,m}\Bigg[\Big(\Omega^{\alpha\beta}_{S;n}-\frac{2g^{\alpha\beta}_{S;n,m}}{\epsilon_{nm}\tau}\Big)\mathcal{J}^{\gamma}_{n}\Big(-\frac{\partial f}{\partial\omega}\Big)_{\epsilon_n}+(\beta\leftrightarrow\gamma)\Bigg] \qquad \text{(D16)}
\end{aligned}$$

$$\begin{aligned}
&\sigma^{\alpha;\beta\gamma}_{\mathrm{dQMD}}\\
&=2\tau\sum_{n,m}\Bigg[\Big(\frac{\epsilon^2_{nm}\tau^2-1}{\epsilon^2_{nm}\tau^2+1}g^{\alpha\beta}_{S;n,m}+\frac{2\epsilon_{nm}\tau}{\epsilon^2_{nm}\tau^2+1}\Omega^{\alpha\beta}_{S;n,m}\Big)\\
&\qquad\times\mathcal{J}^{\gamma}_{n}\mathrm{Im}\Big(-\frac{\partial f}{\partial\omega}\Big)_{\epsilon_n+i\eta}+(\beta\leftrightarrow\gamma)\Bigg] \qquad \text{(D17)}\\
&\simeq\sum_{n}\Bigg[-\Big(\partial^{\gamma}g^{\alpha\beta}_{S;n}\Big)\Big(-\frac{\partial f}{\partial\omega}\Big)_{\epsilon_n}+\frac{2\Omega^{\alpha\beta}_{S;n,m}}{\epsilon_{nm}\tau}\mathcal{J}^{\gamma}_{n}\Big(-\frac{\partial^2 f}{\partial\omega^2}\Big)_{\epsilon_n}\\
&\qquad+(\beta\leftrightarrow\gamma)\Bigg] \qquad \text{(D18)}
\end{aligned}$$

In the limit $\epsilon_{nm}\tau\gg 1$, up to the first order of η, the first term in Eq. (D15) is the conventional Berry curvature dipole term and the second term is the terms pointed out in Ref.[37, 56, 57]. [58] Here, another QMD term emerges from the original Berry curvature dipole term. Because it is the dissipative quantum metric, when there is a band-degeneracy at the Fermi surface, this term also gives the

multi-band correction to the nonlinear Drude term. As same as the smeared QMD term, in the limit $|\epsilon_n-\epsilon_m|\tau \gg 1$, this behaves as almost independent of the strength of the dissipation, while it stems from the dissipation. When considering the limit $\epsilon_{nm}\tau \gg 1$ and approximating $\mathrm{Im}f(\epsilon_n+i\eta)=\eta(\partial f/\partial\omega)|_{\epsilon_n}$, which is enough justified at $\beta\eta \ll 1$, the sum of the smeared QMD term and the first term in Eq. (D18) can be written as,

$$\Big(\partial^\gamma g^{\alpha\beta}_{S;n}+\partial^\beta g^{\alpha\gamma}_{S;n}-\partial^\alpha g^{\beta\gamma}_{S;n}\Big)\Big(\frac{\partial f}{\partial\omega}\Big)_{\epsilon_n}=2\Gamma^{\alpha;\beta\gamma}_{S;n}\Big(\frac{\partial f}{\partial\omega}\Big)_{\epsilon_n}, \tag{D19}$$

where $\Gamma^{\alpha;\beta\gamma}_{S;n}\equiv(\partial^\gamma g^{\alpha\beta}_{S;n}+\partial^\beta g^{\alpha\gamma}_{S;n}-\partial^\alpha g^{\beta\gamma}_{S;n})/2$ can be called the "smeared Christoffel symbol", which is the generalization of the Christoffel symbol in Ref.[45] to the dissipative case. Therefore, we can call the sum of those term as "the smeared Christoffel symbol term" at the Fermi surface.

Finally, we analyze the interband term $\tilde{\sigma}^{\alpha;\beta\gamma}_{\mathrm{Inter}}$ in Eq. (D6).

$\tilde{\sigma}^{\alpha;\beta\gamma}_{\mathrm{Inter}}$ can generate the another Christoffel symbol term and the generalized Berry curvature term as,

$$\sigma^{\alpha;\beta\gamma}_{\mathrm{Inter};1}=\sigma^{\alpha;\beta\gamma}_{\mathrm{ChS:II}}+\sigma^{\alpha;\beta\gamma}_{\mathrm{gBC}}, \tag{D20}$$

$$\begin{aligned}&\sigma^{\alpha;\beta\gamma}_{\mathrm{ChS:II}}\\&=2\sum_{\boldsymbol{k}}\sum_{n,m(\neq n)}\Big[\mathrm{Re}(\mathcal{J}^\alpha_{nm}\mathcal{J}^{\beta\gamma}_{mn})\mathrm{Re}\Big(\frac{1}{(\epsilon_{nm}+2i\eta)^2}\Big)\\&\quad+\Big\{\sum_{l(\neq n)}\mathrm{Re}(\mathcal{J}^\alpha_{nm}\mathcal{J}^\beta_{ml}\mathcal{J}^\gamma_{ln})\mathrm{Re}\Big(\frac{1}{(\epsilon_{nm}+2i\eta)^2(\epsilon_{nl}+2i\eta)}\Big)\Big\}\\&\quad+\Big\{\beta\leftrightarrow\gamma\Big\}\Big]\mathrm{Re}\Big(-\frac{\partial f}{\partial\omega}\Big)_{\epsilon_n+i\eta}+\mathcal{O}(\tau^{-2})\end{aligned} \tag{D21}$$

$$=2\sum_{\boldsymbol{k}}\sum_n g^{\alpha;\beta\gamma}_{S';n}\Big(-\frac{\partial f}{\partial\omega}\Big)_{\epsilon_n}=2\sum_{\boldsymbol{k}}\sum_n\Gamma^{\alpha;\beta\gamma}_{S';n}\Big(-\frac{\partial f}{\partial\omega}\Big)_{\epsilon_n} \tag{D22}$$

$$\simeq\sum_{\boldsymbol{k}}\sum_n\Big(\langle\partial^\alpha n|\partial^{\beta\gamma}n\rangle+\langle\partial^{\beta\gamma}n|\partial^\alpha n\rangle\Big)\Big(-\frac{\partial f}{\partial\omega}\Big)_{\epsilon_n} \tag{D23}$$

$$=2\sum_{\boldsymbol{k}}\sum_n\Gamma^{\alpha;\beta\gamma}_n\Big(-\frac{\partial f}{\partial\omega}\Big)_{\epsilon_n} \tag{D24}$$

$$\begin{aligned}\Gamma^{\alpha;\beta\gamma}_n&=\frac{1}{2}\Big(\partial^\gamma g^{\alpha\beta}_n+\partial^\beta g^{\gamma\alpha}_n-\partial^\alpha g^{\beta\gamma}_n\Big)\\&=\frac{1}{2}\Big(\langle\partial^\alpha n|\partial^{\beta\gamma}n\rangle+\langle\partial^{\beta\gamma}n|\partial^\alpha n\rangle\Big)\end{aligned} \tag{D25}$$

$$\sigma^{\alpha;\beta\gamma}_{\mathrm{gBC}}=\sigma^{\alpha;\beta\gamma}_{\mathrm{gBC:re}}+\sigma^{\alpha;\beta\gamma}_{\mathrm{gBC:im}}+\sigma^{\alpha;\beta\gamma}_{\mathrm{gBC:add}} \tag{D26}$$

$$\begin{aligned}&\sigma^{\alpha;\beta\gamma}_{\mathrm{gBC:re}}+\sigma^{\alpha;\beta\gamma}_{\mathrm{gBC:add}}\\&=2\sum_{\boldsymbol{k}}\sum_{n,m(\neq n)}\Big[\mathrm{Im}(\mathcal{J}^\alpha_{nm}\mathcal{J}^{\beta\gamma}_{mn})\mathrm{Im}\Big(\frac{1}{(\epsilon_{nm}+2i\eta)^2}\Big)\\&\quad+\Big\{\sum_{l(\neq n)}\mathrm{Im}(\mathcal{J}^\alpha_{nm}\mathcal{J}^\beta_{ml}\mathcal{J}^\gamma_{ln})\mathrm{Im}\Big(\frac{1}{(\epsilon_{nm}+2i\eta)^2(\epsilon_{nl}+2i\eta)}\Big)\Big\}\\&\quad+\Big\{\beta\leftrightarrow\gamma\Big\}\Big]\mathrm{Re}\Big(\frac{\partial f}{\partial\omega}\Big)_{\epsilon_n+i\eta}\end{aligned} \tag{D27}$$

$$=\sum_{\boldsymbol{k}}\sum_{n,m(\neq n)}\frac{\Omega^{\alpha,\beta\gamma}_{S';n,m}}{\epsilon_{nm}\tau}\Big(-\frac{\partial f}{\partial\omega}\Big)_{\epsilon_n}+\sigma^{\alpha;\beta\gamma}_{\mathrm{gBC:add}}+\mathcal{O}(\tau^{-2}), \tag{D28}$$

$$\begin{aligned}&\sigma^{\alpha;\beta\gamma}_{\mathrm{gBC:add}}\\&\simeq 2\sum_{\boldsymbol{k}}\sum_{n,m,l(\neq n)}\frac{\mathrm{Im}(\mathcal{J}^\alpha_{nm}\mathcal{J}^\beta_{ml}\mathcal{J}^\gamma_{ln})}{\epsilon^2_{nm}\epsilon_{nl}}\Big(\frac{1}{\epsilon_{nm}\tau}-\frac{1}{\epsilon_{nl}\tau}\Big)\Big(-\frac{\partial f}{\partial\omega}\Big)_{\epsilon_n},\\&\qquad+(\beta\leftrightarrow\gamma)\end{aligned} \tag{D29}$$

$$\begin{aligned}&\sigma^{\alpha;\beta\gamma}_{\mathrm{gBC:im}}\\&=2\sum_{\boldsymbol{k}}\sum_{n,m(\neq n)}\Big[\mathrm{Im}(\mathcal{J}^\alpha_{nm}\mathcal{J}^{\beta\gamma}_{mn})\mathrm{Re}\Big(\frac{1}{(\epsilon_{nm}+2i\eta)^2}\Big)\\&\quad+\Big\{\sum_{l(\neq n)}\mathrm{Im}(\mathcal{J}^\alpha_{nm}\mathcal{J}^\beta_{ml}\mathcal{J}^\gamma_{ln})\mathrm{Re}\Big(\frac{1}{(\epsilon_{nm}+2i\eta)^2(\epsilon_{nl}+2i\eta)}\Big)\Big\}\\&\quad+\Big\{\beta\leftrightarrow\gamma\Big\}\Big]\mathrm{Im}\Big(\frac{\partial f}{\partial\omega}\Big)_{\epsilon_n+i\eta}\end{aligned} \tag{D30}$$

$$=-\sum_{\boldsymbol{k}}\sum_n\frac{\Omega^{\alpha,\beta\gamma}_{S';n}}{\tau}\Big(-\frac{\partial^2 f}{\partial\omega^2}\Big)_{\epsilon_n}+\mathcal{O}(\tau^2), \tag{D31}$$

where the $\Omega^{\alpha,\beta\gamma}_{S';n,m}(g^{\alpha,\beta\gamma}_{S';n,m})$ is the smeared Berry curvature (quantum metric) generalized to the higher-order derivative, which can be derived by the following substitution from $\Omega^{\alpha,\beta\gamma}_{n,m}(g^{\alpha,\beta\gamma}_{n,m})$,

$$\begin{cases}\dfrac{1}{\epsilon^2_{nm}}\to\dfrac{1}{\epsilon^2_{nm}+4\eta^2}\\[2ex]\dfrac{1}{\epsilon_{nm}}\to\dfrac{\epsilon_{nm}}{\epsilon^2_{nm}+4\eta^2},\end{cases} \tag{D32}$$

$$g^{\alpha,\beta\gamma}_{n,m}=\mathrm{Re}\,\langle\partial^\alpha n|m\rangle\langle m|\partial^{\beta\gamma}n\rangle=\Gamma^{\alpha;\beta\gamma}_{n,m} \tag{D33}$$

$$=2\mathrm{Re}\Big[\frac{\mathcal{J}^\alpha_{nm}}{\epsilon_{nm}}\frac{1}{\epsilon_{nm}}\Big(\mathcal{J}^{\beta\gamma}_{mn}+\frac{\mathcal{J}^\beta_{ml}\mathcal{J}^\gamma_{ln}+(\beta\leftrightarrow\gamma)}{\epsilon_{nl}}\Big)\Big] \tag{D34}$$

$$\Omega^{\alpha,\beta\gamma}_{n,m}=2\mathrm{Im}\,\langle\partial^\alpha n|m\rangle\langle m|\partial^{\beta\gamma}n\rangle \tag{D35}$$

If we consider $\partial^{\beta\gamma}$ as the derivative to the new direction, $\Omega^{\alpha,\beta\gamma}_{S';n,m}(g^{\alpha,\beta\gamma}_{S';n,m})$ is also the smeared Berry curvature (quantum metric) generalized to the higher-order derivative. We note that, in two-band systems under the time-reversal symmetry, only the first term in Eq. (D27) can induce the non-reciprocal conductivity $\sigma^{\alpha;\alpha\alpha}$. Under the time-reversal symmetry, the Drude term, the smeared Christoffel term, and the other terms proportional to the

smeared quantum metric are zero. Moreover, the terms proportional to the conventional smeared Berry curvature are also zero because $\alpha = \beta = \gamma$. However, the extended Berry curvature $\Omega^{\alpha,\alpha\alpha}$ can be finite because $\partial^{\alpha\alpha}$ is different from ∂^{α}. As we can see in Eq. (D28), Eq. (D29) and Eq. (D31), this non-reciprocal term under the time-reversal symmetry becomes zero when $\eta \to 0$, which is pointed out in Ref.[18]. Here we also find another necessary condition, which is that the Hamiltonian must have the quadratic term, because $\mathcal{J}^{\alpha\alpha}$ becomes zero without it. Therefore, non-reciprocal transport under the time-reversal symmetry in the DC limit is zero, for example, in the Weyl system with linear dispersion.

[1] J. C. Petersen, M. D. Caswell, J. S. Dodge, I. A. Sergienko, J. He, R. Jin, and D. Mandrus, Nonlinear optical signatures of the tensor order in cd2re2o7 , Nature Physics **2**, 605 (2006).

[2] L. Zhao, D. H. Torchinsky, H. Chu, V. Ivanov, R. Lifshitz, R. Flint, T. Qi, G. Cao, and D. Hsieh, Evidence of an odd-parity hidden order in a spin–orbit coupled correlated iridate, Nature Physics **12**, 32 (2016).

[3] J. W. Harter, Z. Y. Zhao, J.-Q. Yan, D. G. Mandrus, and D. Hsieh, A parity-breaking electronic nematic phase transition in the spin-orbit coupled metal cd2re2o7, Science **356**, 295 (2017).

[4] J. E. Sipe and E. Ghahramani, Nonlinear optical response of semiconductors in the independent-particle approximation, Phys. Rev. B **48**, 11705 (1993).

[5] T. Morimoto and N. Nagaosa, Topological nature of nonlinear optical effects in solids, Science Advances **2**, 10.1126/sciadv.1501524 (2016).

[6] L. Wu, S. Patankar, T. Morimoto, N. L. Nair, E. Thewalt, A. Little, J. G. Analytis, J. E. Moore, and J. Orenstein, Giant anisotropic nonlinear optical response in transition metal monopnictide weyl semimetals, Nature Physics **13**, 350 (2017).

[7] I. Sodemann and L. Fu, Quantum nonlinear hall effect induced by berry curvature dipole in time-reversal invariant materials, Phys. Rev. Lett. **115**, 216806 (2015).

[8] Q. Ma, S.-Y. Xu, H. Shen, D. MacNeill, V. Fatemi, T.-R. Chang, A. M. Mier Valdivia, S. Wu, Z. Du, C.-H. Hsu, S. Fang, Q. D. Gibson, K. Watanabe, T. Taniguchi, R. J. Cava, E. Kaxiras, H.-Z. Lu, H. Lin, L. Fu, N. Gedik, and P. Jarillo-Herrero, Observation of the nonlinear hall effect under time-reversal-symmetric conditions, Nature **565**, 337 (2019).

[9] K. Kang, T. Li, E. Sohn, J. Shan, and K. F. Mak, Nonlinear anomalous hall effect in few-layer wte2, Nature Materials **18**, 324 (2019).

[10] S. Dzsaber, X. Yan, M. Taupin, G. Eguchi, A. Prokofiev, T. Shiroka, P. Blaha, O. Rubel, S. E. Grefe, H.-H. Lai, Q. Si, and S. Paschen, Giant spontaneous hall effect in a nonmagnetic weyl–kondo semimetal, Proceedings of the National Academy of Sciences **118**, 10.1073/pnas.2013386118 (2021), https://www.pnas.org/content/118/8/e2013386118.full.pdf.

[11] B. T. Zhou, C.-P. Zhang, and K. Law, Highly tunable nonlinear hall effects induced by spin-orbit couplings in strained polar transition-metal dichalcogenides, Phys. Rev. Applied **13**, 024053 (2020).

[12] J. W. McIver, D. Hsieh, H. Steinberg, P. Jarillo-Herrero, and N. Gedik, Control over topological insulator photocurrents with light polarization, Nature Nanotechnology **7**, 96 (2012).

[13] C. Kastl, C. Karnetzky, H. Karl, and A. W. Holleitner, Ultrafast helicity control of surface currents in topological insulators with near-unity fidelity, Nature Communications **6**, 6617 (2015).

[14] C.-K. Chan, N. H. Lindner, G. Refael, and P. A. Lee, Photocurrents in weyl semimetals, Phys. Rev. B **95**, 041104 (2017).

[15] A. M. Cook, B. M. Fregoso, F. de Juan, S. Coh, and J. E. Moore, Design principles for shift current photovoltaics, Nature Communications **8**, 14176 (2017).

[16] H. Isobe, S.-Y. Xu, and L. Fu, High-frequency rectification via chiral bloch electrons, Science Advances **6**, 10.1126/sciadv.aay2497 (2020).

[17] X. Zhang, X. F. Ma, Y. Jin, T. Lu, E. P. Boden, P. D. Phelps, K. R. Stewart, and C. P. Yakymyshyn, Terahertz optical rectification from a nonlinear organic crystal, Applied Physics Letters **61**, 3080 (1992), https://doi.org/10.1063/1.107968.

[18] T. Morimoto and N. Nagaosa, Nonreciprocal current from electron interactions in noncentrosymmetric crystals: roles of time reversal symmetry and dissipation, Scientific Reports **8**, 2973 (2018).

[19] Y. Tokura and N. Nagaosa, Nonreciprocal responses from non-centrosymmetric quantum materials, Nature Communications **9**, 3740 (2018).

[20] R. Nakai and N. Nagaosa, Nonreciprocal thermal and thermoelectric transport of electrons in noncentrosymmetric crystals, Phys. Rev. B **99**, 115201 (2019).

[21] R. Wakatsuki, Y. Saito, S. Hoshino, Y. M. Itahashi, T. Ideue, M. Ezawa, Y. Iwasa, and N. Nagaosa, Nonreciprocal charge transport in noncentrosymmetric superconductors, Science Advances **3**, 10.1126/sciadv.1602390 (2017).

[22] Y. M. Itahashi, T. Ideue, Y. Saito, S. Shimizu, T. Ouchi, T. Nojima, and Y. Iwasa, Nonreciprocal transport in gate-induced polar superconductor srtio3, Science Advances **6**, 10.1126/sciadv.aay9120 (2020).

[23] F. Ando, Y. Miyasaka, T. Li, J. Ishizuka, T. Arakawa, Y. Shiota, T. Moriyama, Y. Yanase, and T. Ono, Observation of superconducting diode effect, Nature **584**, 373 (2020).

[24] N. F. Q. Yuan and L. Fu, Supercurrent diode effect and finite momentum superconductivity (2021), arXiv:2106.01909 [cond-mat.supr-con].

[25] A. Daido, Y. Ikeda, and Y. Yanase, Intrinsic superconducting diode effect (2021), arXiv:2106.03326 [cond-mat.supr-con].

[26] J. J. He, Y. Tanaka, and N. Nagaosa, A phenomenological theory of superconductor diodes (2021), arXiv:2106.03575 [cond-mat.supr-con].

[27] Z. Z. Du, C. M. Wang, S. Li, H.-Z. Lu, and X. C. Xie, Disorder-induced nonlinear hall effect with time-reversal symmetry, Nature Communications **10**, 3047 (2019).

[28] S. Nandy and I. Sodemann, Symmetry and quantum kinetics of the nonlinear hall effect, Phys. Rev. B **100**, 195117 (2019).

[29] Z. Z. Du, C. M. Wang, H.-P. Sun, H.-Z. Lu, and X. C. Xie, Quantum theory of the nonlinear hall effect, Nature Communications **12**, 5038 (2021).

[30] T. Morimoto, S. Zhong, J. Orenstein, and J. E. Moore, Semiclassical theory of nonlinear magneto-optical responses with applications to topological dirac/weyl semimetals, Phys. Rev. B **94**, 245121 (2016).

[31] G. B. Ventura, D. J. Passos, J. M. B. Lopes dos Santos, J. M. Viana Parente Lopes, and N. M. R. Peres, Gauge covariances and nonlinear optical responses, Phys. Rev. B **96**, 035431 (2017).

[32] D. J. Passos, G. B. Ventura, J. M. V. P. Lopes, J. M. B. L. d. Santos, and N. M. R. Peres, Nonlinear optical responses of crystalline systems: Results from a velocity gauge analysis, Phys. Rev. B **97**, 235446 (2018).

[33] H. Watanabe and Y. Yanase, Chiral photocurrent in parity-violating magnet and enhanced response in topological antiferromagnet, Phys. Rev. X **11**, 011001 (2021).

[34] H. Watanabe, A. Daido, and Y. Yanase, Nonreciprocal optical response in parity-breaking superconductors (2021), arXiv:2109.14866 [cond-mat.supr-con].

[35] H. Watanabe, A. Daido, and Y. Yanase, Nonreciprocal meissner response in parity-mixed superconductors (2021), arXiv:2109.14874 [cond-mat.supr-con].

[36] Y. Michishita and R. Peters, Effects of renormalization and non-hermiticity on nonlinear responses in strongly correlated electron systems, Phys. Rev. B **103**, 195133 (2021).

[37] Y. Gao, S. A. Yang, and Q. Niu, Field induced positional shift of bloch electrons and its dynamical implications, Phys. Rev. Lett. **112**, 166601 (2014).

[38] D. E. Parker, T. Morimoto, J. Orenstein, and J. E. Moore, Diagrammatic approach to nonlinear optical response with application to weyl semimetals, Phys. Rev. B **99**, 045121 (2019).

[39] Note that, when we consider the anti-symmetric part of $\sigma^{\alpha\beta}$, there is a correction proportional to τ^{-2} to the Hall conductivity due to the imaginary part of the DF.

[40] Here we define the relaxation time $\tau = 1/(2\eta)$ to make the results correspond to the results by the SCB treatment or RDM methods. Although the relaxation time is sometimes defined as $\tau = 1/\eta = 1/(-\mathrm{Im}\Sigma^R)$, this is the relaxation time of the Green function and our relaxation time is the relaxation time of the non-equilibrium distribution function.

[41] In our manuscript, we introduce η phenomenologically by approximating the imaginary part of the self-energy $-\eta$. This approximation represents that we employ the Markov approximation about the relaxation of the single-particle excitation. Under this approximation, the relaxation of the state excited by the electric field with the second order is generally different from that with the first order. On the other hand, in the SCB treatment or RDM methods with the RTA, we approximate any excited states relax with the relaxation time τ. Therefore, it is a more crude approximation than approximating the imaginary part of the self-energy η, and their results correspond to each other only when $\eta \to 0$.

[42] We can see $\sigma_M \propto \eta$ from $(G_n^R - G_n^A)_{i\omega_M} = 2i\eta/((i\omega_M - \epsilon_n)^2 + 4\eta^2)$. We can also see $\sigma_M \propto \eta$ in Fig. 9.

[43] J. Mitscherling, Longitudinal and anomalous hall conductivity of a general two-band model, Phys. Rev. B **102**, 165151 (2020).

[44] J. E. Sipe and A. I. Shkrebtii, Second-order optical response in semiconductors, Phys. Rev. B **61**, 5337 (2000).

[45] J. Ahn, G.-Y. Guo, and N. Nagaosa, Low-frequency divergence and quantum geometry of the bulk photovoltaic effect in topological semimetals, Phys. Rev. X **10**, 041041 (2020).

[46] One can check $\Omega^{\alpha,\beta\gamma}_{n,m} = (\Omega^{\alpha\beta}_{n,m}\mathcal{J}^{\gamma}_{m} + (\beta \leftrightarrow \gamma))/\epsilon_{nm}$ by substituting $l = m$ in Eq. (27).

[47] J. Wilson and A. Yoffe, The transition metal dichalcogenides discussion and interpretation of the observed optical, electrical and structural properties, Advances in Physics **18**, 193 (1969), https://doi.org/10.1080/00018736900101307.

[48] G.-B. Liu, D. Xiao, Y. Yao, X. Xu, and W. Yao, Electronic structures and theoretical modelling of two-dimensional group-vib transition metal dichalcogenides, Chem. Soc. Rev. **44**, 2643 (2015).

[49] S. Kanasugi and Y. Yanase, Multiple odd-parity superconducting phases in bilayer transition metal dichalcogenides, Phys. Rev. B **102**, 094507 (2020).

[50] J. Bezanson, A. Edelman, S. Karpinski, and V. B. Shah, Julia: A fresh approach to numerical computing, SIAM review **59**, 65 (2017).

[51] D. Kaplan, T. Holder, and B. Yan, Unifying semiclassics and quantum perturbation theory at nonlinear order (2022).

[52] T. Matsushita, S. Fujimoto, and A. P. Schnyder, Topological piezoelectric effect and parity anomaly in nodal line semimetals, Phys. Rev. Research **2**, 043311 (2020).

[53] A. Yamakage, Y. Yamakawa, Y. Tanaka, and Y. Okamoto, Line-node dirac semimetal and topological insulating phase in noncentrosymmetric pnictides caagx (x = p, as), Journal of the Physical Society of Japan **85**, 013708 (2016), https://doi.org/10.7566/JPSJ.85.013708.

[54] Y.-H. Chan, C.-K. Chiu, M. Y. Chou, and A. P. Schnyder, ca_3p_2 and other topological semimetals with line nodes and drumhead surface states, Phys. Rev. B **93**, 205132 (2016).

[55] Y. Gao and D. Xiao, Nonreciprocal directional dichroism induced by the quantum metric dipole, Phys. Rev. Lett. **122**, 227402 (2019).

[56] H. Watanabe and Y. Yanase, Nonlinear electric transport in odd-parity magnetic multipole systems: Application to mn-based compounds, Phys. Rev. Research **2**, 043081 (2020).

[57] T. Holder, D. Kaplan, R. Ilan, and B. Yan, Mixed axial-gravitational anomaly from emergent curved spacetime in nonlinear charge transport (2021).

[58] Eq. (13) in Ref.[37] includes a typo. The correct equation should be $\frac{\partial^2 j_i}{\partial E_j \partial E_l} = \int (v_i G_{jl} - v_j G_{li} - v_l G_{ij}) \frac{\partial f_0}{\partial \epsilon_0} \frac{d^3k}{(2\pi)^3}$. The second and third terms correspond to the second term in Eq.(D15) in our paper.